# An adult clock regulator links circadian rhythms to pancreatic β-cell maturation

Ana P. Montalvo Landivar[1,8], Zihan Gao[2,3,4,8], Mai Liu[2,3,4,8], Zoe L. Gruskin[2,3,5], Andrew Leduc[6], Sam Preza[2,3,4], Yu Xie[2,3,4], Andrea V. Rozo[3], June H. Ahn[2,3], Juerg R. Straubhaar[7], Nicolai Doliba[3], Doris A. Stoffers[3], Nikolai Slavov[6], and Juan R. Alvarez-Dominguez[2,3,5,9,*]

[1] Department of Neurosurgery, Brigham and Women's Hospital; Boston, MA 02115, USA.

[2] Chronobiology and Sleep Institute, and Institute for Regenerative Medicine, University of Pennsylvania Perelman School of Medicine; Philadelphia, PA 19104, USA.

[3] Institute for Diabetes, Obesity and Metabolism, University of Pennsylvania Perelman School of Medicine; Philadelphia, PA 19104, USA.

[4] Department of Bioengineering, University of Pennsylvania; Philadelphia, PA 19104, USA.

[5] Department of Cell and Developmental Biology, University of Pennsylvania Perelman School of Medicine; Philadelphia, PA 19104, USA.

[6] Departments of Bioengineering and Biology, Single-Cell Proteomics Center and Barnett Institute, Northeastern University; Boston, MA 02115, USA.

[7] Bioinformatics Center, Massachusetts Eye and Ear Infirmary; Boston, MA 02114, USA.

[8] These authors contributed equally to this work

[9] Lead contact

*Correspondence: Juan.Alvarez@pennmedicine.upenn.edu

**SUMMARY**

The circadian clock attunes metabolism to daily energy cycles, but how it regulates maturation of metabolic tissues is poorly understood. Here we show that DEC1, a clock transcription factor induced in adult islet β cells, coordinates their glucose responsiveness by synchronizing energetic and secretory rhythms. DEC1 binds and regulates maturity-linked genes to integrate insulin exocytosis with energy metabolism, and β-cell *Dec1* ablation disrupts their transcription synchrony. *Dec1*-disrupted mice develop lifelong glucose intolerance and insulin deficiency, despite normal islet formation and intact *Clock/Bmal1* genes. Metabolic dysfunction upon β-cell *Dec1* loss stems from poor coupling of insulin secretion to glucose metabolism, reminiscent of fetal/neonatal immaturity. We link stunted maturation to a deficit in circadian bioenergetics, prompted by compromised glucose utilization, mitochondrial dynamics, and respiratory metabolism, which is rescued by increased metabolic flux. Thus, DEC1 links circadian clockwork to β-cell metabolic maturation, revealing a hierarchy for how the clock programs metabolic tissue specialization.

## INTRODUCTION

Optimizing energy use to fuel availability is critical for metabolic fitness[1,2]. Circadian clocks evolved to anticipate 24-hour cycles in energy availability tied to earth's rotation[3,4]. In mammals, clocks throughout the body optimize critical energy-requiring tasks—from gene expression to protein synthesis—to daily energy cycles by programming cell-autonomous 24-hour rhythms[5,6]. These circadian rhythms emerge as cells differentiate along specific lineages[7,8], yet how they regulate differentiated cells becoming functionally specialized, or "mature", is not understood[9,10].

The circadian clock mechanism comprises a core feedback loop between transcriptional activators (CLOCK/BMAL1) and repressors (PERs/CRYs), along with interlocking regulatory loops involving the ROR, REV-ERB, and DEC transcription factors[11]. These clock regulators play general and specific roles in metabolism, and metabolic effectors in turn provide regulatory feedback to the clock[5,12]. As a result, circadian clockwork shapes and is shaped by myriad metabolic functions—from nutrient uptake and transport to breakdown and storage. Accordingly, clockwork disruption or circadian misalignment fuel obesity, metabolic syndrome, and diabetes in animal models[13-15] and humans[5,16,17]. However, major questions remain as to how the core and interlocking clock regulators coordinate metabolic shifts to enable a mature physiology[6,18].

Pancreatic islet β cells, vital controllers of glucose homeostasis, offer a model to dissect how the molecular clock steers metabolic specialization. The β cell-autonomous clock optimizes glucose-stimulated insulin secretion (GSIS) responsiveness to the active, feeding phase of the day[19,20]. Critically, *Clock*-mutant or *Bmal1*-ablated mice show stunted islet growth and GSIS responsiveness, leading to hypo insulinemic diabetes[15,21,22]. Although the underlying mechanisms are unclear, the CLOCK/BMAL1 complex is thought to modulate GSIS responsiveness by programming rhythmic transcription of late secretory machinery[23].

We previously reported that DEC1 (also called BHLHE40, SHARP2), an understudied clock regulator, is in the core transcriptional regulatory circuit that defines β-cell identity[24]. Here, we define DEC1's targets in β cells and use genetic, single-cell, and biochemical studies to reveal its role in the daily control of insulin secretion and metabolic homeostasis. We find that DEC1 (but not CLOCK/BMAL1) binds and synchronizes the rhythmic transcription of maturity-linked genes integrating energy metabolism and GSIS. *Dec1*-ablated mice are hypo-metabolic and develop lifelong glucose intolerance and insulin deficiency, which we link to immature islet function resulting from poor coupling of insulin secretion to glucose stimulation. Single-cell DNA accessibility, RNA expression, and proteome profiling of *Dec1*-ablated β cells trace this defect to disrupted regulators/effectors of insulin responses to glucose sensing and metabolism. Accordingly, rhythmic glucose import and glycolytic and mitochondrial flux are impaired in *Dec1*-ablated islets, whereas chemical flux stimulation rescues their GSIS deficit. These findings link the β-cell maturation process to circadian optimization of bioenergetics, revealing a modular hierarchy by which the clock programs metabolic tissue specialization.

## RESULTS

### Circadian clock regulator DEC1 defines mature β cells and controls glucose homeostasis

We found that *Dec1* expression discerns mature (juvenile/adult) from immature (fetal/neonatal) β-cells in mouse, rat, pig, and human (Figures 1A and S1A). *Dec1*'s evolutionary conserved selectivity for adult β-cells is second only to *Mafa* (a key driver of mature β-cell physiology[25,26]) among adult-restricted transcription factors that are known to regulate human β-cell maturation.

Physiologic *Dec1* expression in adult mouse β-cells cycles diurnally (Figure 1B), consistent with *Dec1*'s known role in regulating the mammalian circadian clock[27,28]. To determine DEC1's role in metabolism, we examined glucose homeostasis in 2-3-month-old *Dec1*$^{-/-}$ mice[29] and wild-type littermates (Figure 1C). *Dec1*$^{-/-}$ mice show significantly elevated fasting and fed blood glucose (Figure 1D), despite normal islet mass, architecture, and β-cell proliferation (Figures S1B-S1C). *Dec1*$^{-/-}$ mice also display pronounced glucose intolerance at 2-3 months-old (Figure 1E) which persists after 8 months of age (Figure S1F). Importantly, impaired glucose homeostasis in *Dec1*$^{-/-}$ mice is not due to obesity or insulin resistance. Weekly body weight is indistinguishable between *Dec1*$^{-/-}$ and wild-type mice, as is body composition (Figures S1D and S1E). Insulin tolerance tests evidence regular sensitivity to exogenous insulin, which normalizes the elevated blood glucose (Figure 1G). In contrast, *Dec1*$^{-/-}$ mice show significantly impaired glucose-stimulated insulin secretion (GSIS) *in vivo* (Figure 1F), suggesting that compromised metabolism upon *Dec1* loss follows a primary defect in β-cell function.

Together, these findings implicate DEC1 as a rhythmic transcriptional regulator selective for adult β cells that controls physiological glucose homeostasis.

**DEC1 regulates circadian energy expenditure rhythms**

To investigate energy balance, we conducted indirect calorimetry in *Dec1*$^{-/-}$ mice and wild-type littermates under light-dark (LD) and dark-dark (DD) cycles (Figures 2A and 2D). We find that *Dec1*$^{-/-}$ mice keep circadian cycles but are hypo-metabolic, as they spend less energy despite raised cage locomotion. In LD, *Dec1*$^{-/-}$ mice show significantly lower energy expenditure, and a differential effect of mass on energy expenditure, selectively in the dark (active) phase (Figures

2B and 2C). Dark-phase oxygen consumption and carbon dioxide production are reduced relative to wild-type, while food and water intake and the respiratory exchange ratio are unaltered. We verified that activity rhythms remain similar, with no differences in wheel running or overall locomotor activity (Figure 2A). Yet, pedestrian locomotion and distance traveled are increased in the light (inactive) phase (Figures S2A-C). In constant darkness (DD), *Dec1*$^{-/-}$ mice keep daily activity and energy balance rhythms but remain hypometabolic. Energy expenditure rhythms show no significant change in the free-running period length (Figure 2G), but levels remain dulled in the subjective active phase (Figure 2E), whereas the phase exhibits a delayed onset (Figure 2H), consistent with DEC1's known role in tuning circadian phase[30,31]. As with LD cycles, energy expenditure is differently affected by mass (Figure 2F), despite no changes in wheel running or overall locomotor activity levels, while ambulation is increased throughout the day (Figure S2D-F).

Taken together with stable fuel preference and feeding (Figures 2A and 2D), unaltered body mass and composition (Figures S1D-E), and glucose intolerance (Figures 1E and S1F), these phase-dependent changes in energy expenditure and locomotion link DEC1 to the circadian control of energy metabolism.

**DEC1 selectively binds rhythmic energy metabolism and secretory genes in β-cells**

To better understand how DEC1 tunes β-cell function, we examined its genome-wide binding by chromatin immunoprecipitation-sequencing in unsynchronized mouse β-TC6 cells (Figures 3A), along with that of homolog DEC2 (also called BHLHE41, SHARP1) (Table S1). As expected, DEC1 and DEC2 bind CACGTG E-box motifs with significant overlap, mainly at promoters,

including those of core clock activators (*Clock/Bmal1*), repressors (*Per*/*Cry*), and interlocking loop (*Ror*, *Rev-erb*, *Dec*) genes (Figures S3A-E). Among sites bound by DEC1 and DEC2, 26% (2,179) are also bound by CLOCK/BMAL1 in Beta-TC6 cells[23], consistent with competition for E-box binding[28], and enrich for circadian clock and NOTCH/TGF-β signaling effectors (Figures 3A, 3B, and S3F). Surprisingly, the non-overlapping DEC1/DEC2 and CLOCK/BMAL1 binding sites target largely distinct gene pathways, with β-cell development regulators selectively bound by DEC1 (Figures 3A and S3E). The DEC1/DEC2-specific cistrome enriches for (i) key maturity controllers like *Neurod1* and *Mafa*[25,32]; (ii) energy metabolism effectors like *Glut2* and *ChREBP* that enact β-cell glucose import[33] and mitogenic signaling[34]; and (iii) components of insulin signaling (*Insr, Irs1, Igf2*) and of vesicle membrane docking/fusion, including many voltage-gated K/$Ca^{2+}$ channel subunits, calmodulins/$Ca^{2+}$-dependent kinases, and SNAREs (*Vamp2/3, Stx4a/6/16, Stxbp1/5l/6, Snap25/91/in*). By contrast, CLOCK/BMAL1-specific targets enrich for late secretory genes, including cAMP-coupled signaling mediators of vesicle budding, consistent with impaired cAMP-mediated stimulation of insulin release in *Bmal1*-disrupted mice[23].

DEC1/DEC2 and CLOCK/BMAL1 may cooperate with distinct co-factors to bind distinct E-boxes. For example, sites bound by CLOCK/BMAL1 but not DEC1/ DEC2 are often co-bound by the pancreatic lineage-determining factor PDX1[23] (Figure 3A). We thus examined transcription factor binding motifs enriched at DEC1/DEC2-only and CLOCK/BMAL1-only binding sites. We find that DEC1/DEC2-only sites enrich for binding motifs of E-box binding metabolic regulators (HIF1A, ChREBP, MAX), while CLOCK/BMAL1-only sites enrich for those of β-cell development regulators (PDX1, NKX6.1, PAX6, HNF1A/6) (Figure S3G). This suggests a basis for modular control of β-cell clock outputs, where CLOCK/BMAL1 team with pancreatic lineage-determining factors to selectively target late secretory genes, while

DEC1/DEC2 preferentially team with E-box binding metabolic regulators to target energy metabolism/signaling mediators of insulin responses to glucose.

To test rhythmicity among DEC-bound gene targets, we performed RNA-sequencing around the 24-hour clock in islets from wild-type mice and used dryR[35] for Bayesian statistics-based rhythm model selection. DEC1/DEC2 targets show pervasive 24-hour cycling, comprising ~73% of bound and expressed genes, comparable to ~72% for CLOCK/BMAL1 targets, which co-varied in rhythm amplitude and significance values (Figures 3C and S3H). Notably, rhythmic DEC1 targets include regulators of β-cell function, energy metabolism, and insulin secretion (see below) known to oscillate in human islets[23,24,36].

Together, these findings argue that DEC1 regulates GSIS at specific steps, by selectively binding rhythmic genes mediating glucose and insulin metabolism, revealing a hierarchy for how distinct clock factors link to the physiology of adult β-cells.

**β-cell DEC1 loss causes insulin deficiency and glucose intolerance due to islet immaturity**

We next sought to ascertain the direct role of β-cell DEC1 in metabolic homeostasis by creating *InsCre Dec1*$^{flx/flx}$ (hereafter *βKO*) mice. The mice display normal islet anatomy, number, β-cell proliferation, and insulin content, despite DEC1 loss (Figures 4A and S4A-F). Yet, 3-4-month-old *Dec1-βKO* mice develop striking glucose intolerance compared to wild-type or heterozygous littermates specifically in the rest phase (Figure 4B), when *Dec1* normally peaks (Figure 1B). As with *Dec1*$^{-/-}$ mice, glucose intolerance persists in 8-month-old *Dec1-βKO* animals (Figure S4G). While weight and insulin sensitivity are normal (Figures S4H and S4I), *Dec1-βKO* mice are hypo-insulinemic, as indicated by reduced *ad libitum* and glucose-stimulated blood insulin levels

mainly in the rest phase (Figures 4C and S4J). Further, *Dec1-βKO* islets show stunted GSIS magnitude and kinetics in static and dynamic assays (Figures 4D and S4K). Thus, β-cell *Dec1* loss severely hampers islet GSIS, rendering mice glucose intolerant.

Islets develop mature GSIS after birth, marked by increases in the glucose threshold for insulin release and the glucose-coupled release capacity[37,38]. To define the defective step in *Dec1-βKO* islet GSIS, we tested their responses across increasing glucose levels in static and dynamic incubations. Isolated *Dec1-βKO* islets show elevated insulin secretion under sub-physiological glucose, mounting anomalous insulin responses between 0.5mM and 2.8mM glucose and between 2.8mM and 5mM glucose (Figures 4E and S4K-L). This indicates a lower glucose threshold for insulin release, reminiscent of fetal/neonatal islets[37,38]. By contrast, insulin responses to physiological (8mM) and saturating (20mM) glucose levels are diminished in *Dec1-βKO* islets, despite normal insulin content and release upon chemical depolarization with KCl (Figures 4D-E, S4F, and S4K-L). This indicates blunted glucose-coupled insulin release capacity.

Collectively, these findings reveal that β-cell *Dec1* disruption results in insulin deficiency owing to functionally immature glucose responsiveness.

**DEC1 synchronizes metabolic and insulin secretion gene rhythms in β cells**

To assess how DEC1 regulates mature GSIS function, we examined the impact of β-cell *Dec1* loss on islet gene expression patterns. RNA-sequencing over a 24-hour cycle in islets isolated from *Dec1-βKO* mice revealed 3,176 genes (13% of all detected) with differential rhythms (Figures 5A, S5A; Table S2). Rhythm-disrupted genes enrich for functions in vesicular transport and epigenetic regulation (Figure 5A). These genes include *Bmal1* (Figure 5E), although other

core clock genes that are also bound by DEC1 lack significant rhythm changes (Figure S5F). We also found 818 genes that gain a 24-hour rhythm, enriching for calcium signaling mediators and general machinery for vesicle budding. Cycling amplitudes of rhythm-disrupted and -acquired genes are globally greater than those of rhythm-retaining genes (Figure S5A), supporting their *bona-fide* rhythmicity. Unexpectedly, many GSIS regulators retained daily cycling but became phase shifted (Figures 5A-5C and S5C-S5E). These include (i) effectors of glucose sensing (*Glut2*, *Foxo1*) and mitochondrial metabolism (TCA, electron transport chain, ATP synthesis enzymes); (ii) PI3K-Akt-mTOR signaling modulators of energy homeostasis (*Gsk3b, Igf1*); and (iii) direct effectors of insulin transport (tubulins, ARF/RAB GTPases) and exocytosis (G-protein subunits, *Irs1/2, Syt4/13*). Disparate phase shifts include phase advances for electron transport chain components and phase delays for the *Glut2*/*Igf1* effectors of glucose sensing (Figures 5B-C, S5D-E, and S5G). Globally, phase offsets between respiratory metabolism and GSIS gene rhythms are lost in *Dec1-βKO* islets (Figure S5D), indicating time desegregation of metabolic processes. DEC1 binding is enriched among rhythm-shifted genes (Figures 5D and S5B), consistent with a role in coordinating the oscillation phase of direct targets[31].

Together, these finding indicate that temporal gene control by DEC1 in mature β cells serves to synchronize insulin responses to glucose sensing and oxidative metabolism.

**DEC1 regulates coupling of insulin secretion to glucose, shaping islet cell-cell coordination**

Islets rely on temporally orchestrated interactions of heterogeneous cell types to sustain glucose homeostasis[39,40]. To better understand cell type-specific effects in *Dec1-βKO* islets, we subjected them to single-cell RNA sequencing (scRNA-seq), single-cell assay for transposase-accessible

chromatin by sequencing (scATAC-seq), and single-cell proteomic mass spectrometry (SCoPE-MS)[41,42]. Marker-based cross-modal integration[43] clearly identified endocrine (α, β, δ, γ), vascular, stellate, and immune cells (Figures 6A, S6A, and S6B). We further discerned as endocrine cell subpopulations (i) β1/β2 cells with higher/lower expression of insulin and the maturity markers *Ucn3*[37] and *Iapp*[44]; (ii) α1/α2 cells with higher/lower glucagon and *Irx2, Arx*; (iii) δ1/δ2 cells with higher/lower somatostatin and *Hhex*. We find that β1 cells are significantly depleted in *Dec1-βKO* islets (Figure S6A), while overall endocrine cell type ratios remain intact, evidencing selective loss of β cells in functionally mature states.

Analyzing RNA changes across *Dec1-βKO* islet cell groups reveals pervasive gene deregulation, with ~40% of changes equally ascribed to β1 and β2 cells (Figure S6C). Overlap of RNA and ATAC changes across β cells further reveals concurrent chromatin and expression-level deregulation of shared gene sets, enriched for functions in GSIS regulation (Figures 6A and S6D-E). Critically, these changes remodel the proteome, as SCoPE-MS single-cell proteomics unveils significant deregulation of proteins mediating glucose metabolism (TCA, OXPHOS enzymes) and GSIS (insulin processing, transport, and secretion) in β cells (Figures 6B and S6G-H). To identify subsequent effects on intercellular signaling, we focused on ligand-receptor interaction changes where the ligand is altered in β1 cells, given their marked downregulation (Figures 6C and S6F). As expected, we find reduced insulin signaling from β1 cells (to themselves and to δ cells). This is accompanied by reduced signaling of the WNT4 maturity modulator[45], the JAM2/3 junction adhesion proteins, and the NRNX1 secretory granule co-regulator from β1 to other endocrine cells, while ligand activity of the APP amyloid beta precursor protein is enhanced. These results offer a molecular basis for how GSIS deregulation in β cells disrupts intercellular coordination in *Dec1-βKO* islets.

We next studied the impact of altered gene expression on rhythmicity in *Dec1-βKO* islets. Most differentially expressed genes either lack or retain rhythmicity (Figure S6I). Yet, specific subsets, enriched for GSIS effectors, change in both rhythm and mean expression level, with exocytic machinery concurrently upregulated and phase-shifted in rhythm (Figure S6J). To establish direct transcriptional regulation by DEC1, we intersected differentially expressed and rhythm-altered genes with the DEC1 cistrome (Table S2). This identified 25 DEC1 targets that specifically enrich for roles in glucose responsiveness and insulin secretion (Figures 6D and 6E; Table S3). Remarkably, 5 such targets influence both insulin release and glucose responsiveness: (i) the key β-cell maturity transcription factors *Mafa*[25,26] and *Hif1a*[46]; (ii) the exocyst co-factor *Wash1c*[47]; and (iii) the $G_o$-type G protein–coupled receptor subunit *Gnao1* and the *Abr* RhoGEF and GTPase activator.

Together, these findings reveal the direct DEC1 targets that link glucose responsiveness to insulin discharge, delineating the core pathway for DEC1's control of adult β-cell function.

**A deficit in circadian bioenergetics underlies immature β-cell function upon DEC1 loss**

Given DEC1's selective binding and circadian regulation of energy metabolism genes, we next tested its influence on cellular energetics. We find that DEC1 is vital for time-of-day variation in GSIS reponsiveness[23,48] (Figure 7A). Importantly, this reflects a critical requirement for circadian mitochondrial energetics. Mitochondrial fusion into tubular networks enabling higher oxidative activity is under circadian control[49], and day-to-night switching from fragmented (spherical) to tubular (branched) mitochondria is blunted in *Dec1*-ablated β-cells, despite stable mitochondrial content (Figures 7B, S7A and S7B). Mitochondrial volume, surface area, and branching (number,

length, junctions, and endpoints) are significantly higher than wild type, while sphericity is lower, in the subjective rest phase specifically (Figure S7A). In line with stunted mitochondrial dynamics, circadian cycling of cellular reactive oxygen species dulls in DEC1's absence (Figure S7C). These defects coincide with marked declines in the active phase rise in cells with high mitochondrial membrane potential (MMP) and in maximal MMP (Figures 7C and S7D). Direct oxygen consumption measurements reveal that *Dec1* loss significantly stifles basal, glucose-stimulated, ATP-linked, and maximal respiration, hindering spare respiration capacity, mainly in the subjective rest phase (Figures 7D and S7E). Thus, DEC1 is critical for circadian rhythms in mitochondrial activity and in GSIS responsiveness.

Reduced mitochondrial dynamics and respiration in DEC1's absence may reflect adaptations to reduced glucose utilization. We find that rest-phase glycolysis rates are indeed markedly stifled, while non-glycolytic acidification is elevated in the active phase (Figures 7D, 7E, and S7F). We thus tested if curbed reliance on glucose upon *Dec1* loss reflects lower glucose import. Uptake of a fluorescent glucose analog was markedly lower in the rest phase, and the active phase rise in cells with high uptake was severely disrupted (Figure 7F). Taken together with compromised glycolysis, mitochondrial dynamics and oxidative respiration, these data reveal that immature GSIS upon DEC1 loss is due to a deficit in circadian glucose metabolism.

We next conducted a targeted screen of insulinotropic agents to rescue the GSIS defect of isolated *Dec1*$^{-/-}$ and *Dec1-βKO* islets (Figures 7G-H and S7G-H). Glucose stimulation along with cAMP agonists forskolin or 8-br-cAMP fails to rescue the significant GSIS deficit, as does co-stimulation with ionomycin, a $Ca^{2+}$ ionophore, consistent with normal $Ca^{2+}$ influx dynamics (Figure S7G). Conversely, glucose-independent stimulation with PMA (phorbol 12-myristate 13-acetate), a direct PKC activator, or with carbachol, a muscarinic receptor agonist, restores insulin

secretion to wild-type levels (Figures 7H and S7H). To rescue the specific defect in glucose coupling of insulin release, we then sought to increase metabolic flux. Raising the pyruvate pool with TEPP-46, a pyruvate kinase activator, or the acetyl-CoA pool with DCA (dichloroacetate), a pyruvate dehydrogenase kinase inhibitor, dramatically boosts GSIS beyond wild-type activity (Figure 7H). Similarly, enhancing glycolytic flux with dorzagliatin, a glucokinase activator, improves GSIS beyond wild-type levels. Thus, greater energy flux relieves the hypo-metabolic cellular state caused by *Dec1* loss, revealing a molecular path for DEC1's impact on β-cell metabolic maturation and systemic glucose homeostasis.

## DISCUSSION

We have defined a genomic basis for the coordination of metabolism by adult β cell-specific circadian clockwork. Tissue-intrinsic physiology rhythms are thought to be programmed by the ubiquitous CLOCK/BMAL1 activators partnering with lineage-restricted transcription factors[4,50], consistent with the phenotypes of conditional CLOCK/BMAL1 knockouts. Yet, not all rhythmic genes are CLOCK/BMAL1 targets, and such knockouts may lack the entire circadian system[6]. Using pancreatic β-cells as a model for cell type-specific circadian control of metabolism, we identify discrete roles for the ubiquitous CLOCK/BMAL1 complex and the adult-restricted DEC1 regulator in programming energy metabolism and secretory gene oscillations that drive diurnal variation in the glucose responsiveness of insulin secretion.

Our genomic binding studies illuminate how tissue-specific clock outputs are generated. Both CLOCK/BMAL1 and DEC1/DEC2 target E-box motifs and bind clock genes, including each other's, but most of their binding targets are distinct. CLOCK/BMAL1 preferentially binds

sites co-targeted by pancreatic lineage-determining factors like PDX1[23], enriched for late secretory genes. By contrast, DEC1/DEC2 selectively bind metabolic/signaling mediators of insulin responses to glucose, co-targeted by energy metabolism regulators like HIF1A and ChREBP. As both sets of target genes show robust rhythms, our results reveal a hierarchy for controlling clock outputs, with cell state-specific gene rhythms set mainly by interlocking loop controllers, rather than core clock components directly[51,52]. This model does not exclude indirect effects, as core clock and interlocking loop controllers regulate each other. Further studies will be needed to determine the basis for these factors targeting distinct E-boxes within the same cell type or across diverse tissues[53,54].

Our discovery that *Dec1* loss suffices to cause lifelong glucose intolerance and insulin deficiency, as with pancreas/β-cell *Bmal1* loss but without stunted islet growth or survival[15,55], argues that circadian GSIS control operates mainly through this arm of the clock. We further find that *Dec1* loss renders islets refractory to glucose at least in part due to a diminished threshold for insulin release, as with fetal/neonatal islets[37,38]. Given DEC1's adult-specific induction and direct control of β-cell maturity genes like MAFA, these findings uncover a molecular link between the circadian system and development of the mature β-cell phenotype.

Mechanistically, we show that DEC1-mediated synchrony of energy metabolism rhythms is vital to coordinate the specialized physiology of β-cells. Such role is consistent with DEC1's ability to entrain circadian rhythms to environmental stimuli[27,31]. Indeed, we find that energy expenditure and activity rhythms show delayed phase onset in *Dec1*$^{-/-}$ mice. We further detect altered phase alignment in the expression rhythms of oxidative metabolism and insulin secretion effectors. Temporal segregation of incompatible metabolic processes is key for optimized cell and tissue physiology[1,2], and we find that phase dysregulation leads to circadian deficits in

glucose utilization, mitochondrial respiration, and GSIS. We also show that DEC1-mediated control of mitochondrial dynamics, which are known to undergo circadian regulation[49], is important for optimizing β-cell metabolic function.

Optimizing tissue functions to energy availability offers a clear fitness advantage[1,2]. As circadian clocks emerge in metabolic tissues during the onset of daily feeding-fasting cycles[56,57], an intriguing possibility is that they unlock phenotypic maturity by optimizing specialized tasks to daily energy availablity[9]. Lapses in such circadian optimization, as occurs with chronic circadian rhythm disruption[5,16], may thus lead to multi-tissue dysfunction due to a broad loss of mature cell phenotypes.

Overall, our finding that insulin secretion's responsiveness to glucose relies on DEC1-driven synchrony of circadian metabolic and secretory rhythms illuminates how adult β-cells achieve specialized function. Given major interest in achieving maturation of *in vitro*-derived human islets for diabetes modeling and therapy[58,59], the fact that DEC1 marks mature β-cells from rodents to human heralds new paths to co-opt bioenergetic rhythms to realize fully functional lab-grown β-cells for research and medicine.

## ACKNOWLEDGEMENTS

We thank Douglas A. Melton for his generous support during the initial stage of this project, and Daria Zhadanova, Monica Cho, Israeli M. Galicia-Silva, Samuel D. Pollock, and Azariah Wise for assistance with data analysis and graphics; the Beth Israel Deaconess Medical Center Metabolic Core, Harvard Medical School Biopolymers Facility, Harvard University Bauer Core sequencing facility, and the University of Pennsylvania Laboratory Animal resources, Diabetes

Research Center Islet Cell Biology Core, and Cell and Developmental Biology Microscopy Core for technical support and critical discussions; and Mitchell A. Lazar, Amita Sehgal, Kenneth S. Zaret and members of the Alvarez-Dominguez laboratory for critical feedback on this manuscript. This work was supported by grants from the NIH (K01DK129442), the Human Islet Research Network (U24DK104162), start-up funding from the Perelman School of Medicine at the University of Pennsylvania, and by a pilot award from the Diabetes Research Center at the University of Pennsylvania (P30DK19525) to J.R.A-D., who was also supported by a Howard Hughes Medical Institute Life Sciences Research Foundation Fellowship; and by grants to Douglas A. Melton from the JDRF (5-COE-2020-967-M-N), and the JPB Foundation (award no. 1094).

## AUTHOR CONTRIBUTIONS

A.P.M.L., Z.G., Z.L.G., A.L., S.A.P., Y.X., A.V.R., and J.RA.-D. performed experiments. M.L., A.L., J.H.A., J.R.S., and J.RA.-D. conducted bioinformatics analyses. A.P.M.L., Z.G., M.L., Z.L.G., N.D., D.A.S., N.S., and J.RA.-D. designed the research, interpreted the results, and wrote the manuscript.

## DECLARATION OF INTERESTS

The authors declare that they have no competing interests.

## STAR METHODS

## LEAD CONTACT AND MATERIALS AVAILABILITY

Further information and requests for resources and reagents should be directed to the Lead Contact (Juan.Alvarez@pennmedicine.upenn.edu). This study did not generate new unique reagents.

## EXPERIMENTAL MODEL AND SUBJECT DETAILS

### Animals

Male *Dec1*$^{-/-}$ mice[29] used in this study were produced and maintained on a C57BL/6J background. *Dec1*$^{f/f}$ mice (kindly provided by Dr. Lino Tessarollo, National Institutes of Health)[29] were crossed to *InsCre* mice (kindly provided by Dr. Douglas Melton, Harvard University)[60] to produce the male *InsCre Dec1*$^{f/f}$ mice and littermate controls used in this study. Unless otherwise noted, all mice were housed on a 12-hours light:12-hours dark cycle (lights on at 6am [zeitgeber time 0, ZT0] and lights off at 6pm [ZT12]) with continuous access to regular chow and water. All animal care and use procedures followed the guidelines of the Institutional Animal Care and Use Committee of the University of Pennsylvania in accordance with the guidelines of the NIH.

## METHOD DETAILS

### Glucose/insulin measurements

Blood glucose levels were measured via tail vein bleed using a OneTouch Ultra2 glucometer (LifeScan). Plasma samples were collected via tail vein bleed into a Microvette CB300 (Sarstedt,

Inc.) capillary tube. Insulin concentration was quantified using a Mouse Ultrasensitive Insulin ELISA kit (ALPCO Diagnostics; 80-INSMSU) within 24 hours of sample collection.

**Glucose and insulin tolerance tests**

Glucose tolerance tests were conducted in mice fasted for 14 hours. Blood glucose levels were measured as indicated above following intraperitoneal injection of room-temperature D-(+)-glucose in 0.9% sterile saline at 2g/kg of body weight. Plasma insulin was measured as indicated above. Insulin tolerance tests were performed after a 4-hour fast, followed by intraperitoneal injection of 4°C insulin (*Humulin R*, Eli Lilly) in 0.9% sterile saline at 1U/kg of body weight.

**Indirect calorimetry**

Indirect calorimetry measurements were collected as described[61] with mice housed at 23°C in Promethion indirect calorimetry cages (Sable Systems) with free access to food and water. Mice were first assayed under regular light-dark cycles, with 6am-6pm light photoperiod. The first full 24-hour day was considered as an acclimation period, and the following 3 days used for data collection. Lights were then turned off in the chambers for dark-dark cycle measurements over 7 days, with food shaken down in days 2 and 4 at ZT4. Body mass was measured before and after the experiment, and the average was used for regression analyses. Body mass composition was assessed by magnetic resonance imaging with an EchoMRI instrument before placing mice into metabolic cages. CalR analysis (RRID:SCR_015849) was performed as described[61].

**Immunostaining**

Immunostaining was performed as described previously[24]. Mouse pancreata were fixed in 4% paraformaldehyde overnight at 4°C and kept in 70% ethanol. Fixed tissue was sectioned by the Penn Molecular Pathology and Imaging Core (RRID: SCR_022420). Sections were deparaffinized using Histoclear (Thermo Fisher Scientific; C78-2-G), submerged in 1X Citrate buffer (Sigma Aldrich; C9999-1000ML) for antigen retrieval, and placed in a pressure cooker for 30 minutes. Slides were blocked with 5% Donkey Serum (Jackson Immunoresearch; 017-000-121) and PBST (PBS and 0.3% Triton X-100 [Sigma Aldrich]) for 1 hour, then incubated with primary antibodies (Insulin: GB13121, Servicebio; Glucagon: GB13097, Servicebio; Ki67: 14-5698-82, eBioscience) diluted in PBST overnight at 4°C. The next morning, slides were washed twice with PBST and incubated with secondary antibodies at 1:500 dilution in PBST for 1 hour protected from light. Slides were subsequently washed twice and stained with 1x Trueblack (Biotium; 23007) for 1 minute, followed by washing and incubating with PBS for 5 minutes. For imaging, slides were mounted with Prolong gold Antifade mount and with DAPI (Thermo Fisher Scientific; P36935), covered with coverslips and sealed with nail polish. Images were taken using a Zeiss LSM 510 microscope (Carl Zeiss).

**Image analysis**

ImageJ (NIH) was used to evaluate islet area, α and β cell area and relative proportions, and β cell proliferation. Islet area was calculated per $mm^2$ of pancreatic section area. α/β cell proportions were quantified as the fraction of Glucagon+/Insulin+ cells per islet, respectively. To quantify proliferating β cells, we calculated the ratio of Insulin+ Ki67+ cells to total Insulin+ cells within islets.

**Islet isolation**

Islet isolation was conducted as previously described[62], via *in situ* pancreas perfusion with 0.8 mg/ml collagenase P (Roche; 11-213-873-001) followed by pancreas digestion and islet purification using Histopaque 1077 and 1119 (Sigma). Islets were filtered through a 250 µm mesh filter, collected in a 40 µm mesh filter, and manually picked with a 200 µL micropipette, followed by overnight recovery in a 37°C 5% CO2 incubator prior to downstream experiments.

**ChIP-sequencing**

Chromatin immunoprecipitation-sequencing was conducted as described[24], by incubating Beta-TC6 cells (ATCC; CRL-3605) cultured in DMEM supplemented with 15% FBS, 1% L-glutamine, and 1% penicillin/streptomycin with DEC1 (Novus Biologicals; NB100-1800) and anti-V5 (abcam; ab15828), for DEC2-V5 (GeneCopoeia, Inc. # EX-A4343-LX304), antibodies. Sequencing reads were mapped using STAR[63] with default parameters. Regions enriched for uniquely-mapped reads relative to input sample were called as binding peaks using MACS[64] with default parameters and "--pvalue=1e-9 --keep-dup=1", followed by filtering against overlap with problematic regions of the genome[65]. Peaks from BMAL1, CLOCK, and PDX1 ChIP-sequencing in Beta-TC6 cells[23] were called in the same manner and concatenated and merged with DEC1 and DEC2 peaks using BEDTools[66] to obtain a unified peak catalog. Reads in peaks from the unified catalog were quantified using HTSeq[67] in ''-m union'' mode, and normalized as counts per million mapped reads (CPM). K-means clustering was conducted in R (kmeans function) as described[24].

**Motif enrichment**

DNA sequences of DEC1 and DEC2 binding peaks were searched for enriched motifs from a database of vertebrate transcription factor recognition motifs[68-70] using MEME-ChIP [71] under Discriminative mode, which implements CentriMo[72] to identify centrally enriched motifs and tests for similarity to known motifs using Tomtom[73]. Markov models of sequence nucleotide composition were used as the background model for motif matching to normalize for biased distribution of individual letters in the examined sequences. We used FIMO[74] as described[24] to search clusters of peaks from the unified peak catalog for matches to the database of vertebrate transcription factor recognition motifs.

**Pathway enrichment**

Gene lists ranked by a feature of interest (e.g., expression change, -log10 p-value of rhythmicity) were analyzed for enrichment of gene sets grouped by ontology annotations using Metascape[75] with default parameters, followed by curation of a representative term for each ranked annotation term cluster. Genomic regions of interest (e.g. clusters of peaks from the unified peak catalog) were analyzed for enrichment of associated gene ontologies using HOMER[76] with default settings, followed by p-value based ranking and curation to prune redundant terms.

**RNA-sequencing and differential expression**

RNA-sequencing was conducted as described[24]. Sequencing reads were mapped using STAR[63] with default parameters. Read counts per gene were determined using HTSeq[67] and normalized using DESeq[77]. We compared gene expression distributions (regardless of rhythmicity) between *Dec1 βKO* and wild-type islets using dryR[35] (see below) to identify genes with differences in

mean expression level, and considered genes with DESeq p <0.05 in both the islet-level 24-hour time series and the β cell-level scRNA-seq data (see below) to be differentially expressed.

**Rhythmicity analysis**

RNA-sequencing data from *Dec1 βKO* and wild-type islets was analyzed for 24h rhythmicity using dryR[35], which employs a Bayesian information criterion for rhythm and mean expression model selection, considering only genes with cumulative expression >10 normalized counts across the 24-hour time series of either genotype. Default parameters were used to detect and estimate changes in amplitude, peak phase, and mean expression level between the two 24-hour series of N =7 time-points with n =4 replicate measurements each. To establish statistical confidence for a single condition, we used the "dryseq_single" function to compute a p value for each gene. To quantify and compare rhythm phase shifts between *Dec1 βKO* and wild-type islets for gene biological processes, we used PSEA[78], employing a significance threshold of q <0.05 against a uniform phase distribution. Other features of interest (e.g. mitochondrial structural and functional measurements) were analyzed for 24h rhythmicity using RAIN[79], which employs non-parametric Mann-Whitney U tests to compare the ranks of measured values against those of alternative waveforms without assumptions about waveform shape or symmetry and computes a Benjamini-Hochberg corrected p value for each feature. Default parameters and "method = independent" were used to estimate peak phase, shape, and significance from the time series sampling independent populations. Comparable trends and statistical significance estimates were obtained using parametric methods such as harmonic regression. For plotting, time series measurements were detrended by subtracting a linear regression fit, maintaining relative scaling proportions by considering the means and SEMs of both genotypes.

**Islet glucose-stimulated insulin secretion**

Insulin secretion assays were conducted in mouse islets after an overnight recovery from isolation as previously described[24]. 20 size-matched islets were allotted into four groups for triplicate GSIS assays plus insulin content determination, washed with Krebs buffer containing basal (0.5/2.8mM) glucose and loaded into 24-well plate inserts (Millicell Cell Culture Insert; PIXP01250), followed by pre-incubation in Krebs buffer with the same basal (0.5/2.8mM) glucose level for 1h to remove residual insulin. Subsequently, islets were sequentially challenged with Krebs buffer containing indicated glucose concentrations with or without insulinotropic agents, with a 1h incubation for each treatment. For chronic rescue, insulinotropic agents were used to treat overnight-recovered mice islets for 24 hours before the GSIS assay. Insulinotropic agent dosages were: 10μM Ionomycin (STEMCELL; 73722); 10μM Forskolin (Stemolecule; 04-0025); 1mM 8-Br-cAMP (VWR; 80050-494); 1mM Carbachol (Santa Cruz; sc-202092); 10μM PMA (Santa Cruz; sc-3576B); 10μM Dorzagliation (Selleckchem; S6921); 10μM TEPP-46 (ML265) (Selleckchem; S7302); 3μM Cyclosporin A (Enzo; BML-A195-0100) or 1mM DCA (Selleckchem; S8615). After GSIS assays, islets were dissociated using TrypLE Express (Life Technologies) and cell counts were obtained using an automated cell counter (Beckman Coulter; Vi-Cell). For insulin content determination, islets were directly dissolved in M-PER protein extraction reagent (Thermo; 78501). GSIS incubations were conducted at 37ºC with 5% $CO_2$, with supernatant samples collected after each incubation.

Dynamic GSIS of handpicked, size-matched islets was conducted in triplicate as previously described[24] using an automated Perifusion System (BioRep). Chambers were first perifused with Krebs buffer containing basal (0.5/2.8mM) glucose for 1h at a flow rate of

100ul/min and sequentially with the indicated solutions for the indicated durations. Dynamic insulin secretion measurements were normalized to the mean of the first (basal) incubation.

**Single-cell RNA and ATAC-sequencing**

Isolated islets were dissociated using Accutase (StemCell Technologies), followed by single-cell capture, lysis, and RNA/ATAC library preparation with the 10x Chromium system (10x Genomics) using Single Cell 3' Gene expression (v3)/ATAC reagents following the manufacturer's instructions. Libraries were sequenced on a NovaSeq 4000 instrument (Illumina) and aligned to the mm10 reference genome assembly using Cell Ranger (10x Genomics) RNA/ATAC pipelines. Mapped RNA reads were processed as described previously[80] according to guidelines from[81] using Seurat V3[43]. ATAC reads were processed as described[82], filtering against low-quality fragments and excluding regions within non-standard chromosomes or with extremely high (top 2%) nucleosome signal, to minimize noise and artifacts. Principal component analysis was performed on log-scaled counts for the top 2000 highly variable genes, and uniform manifold approximation and projection (UMAP) was computed with the top 50 principal components. Clusters were inferred using the Seurat "FindClusters" function adjusting for cluster resolution to optimize balance between cluster granularity and separation. Cross-modal integration of RNA and ATAC data was performed with Seurat[43] using the "FindTransferAnchors" and "TransferData" functions with a Canonical Correlation Analysis (CCA) dimension reduction method to transfer cluster identities from RNA to ATAC data. Cell clusters were assigned to cell types based on established islet cell identity markers[43].

Gene expression / promoter accessibility were computed for each cell type as expected counts within gene models / promoter-proximal (TSS ± 2kb) regions using RSEM[83]. Differential expression / promoter accessibility was evaluated in β-cells as described[84] using edgeR[85]. Uniquely-mapped reads were removed for duplicates and used for peak calling as described [24] using MACS2[64] with default parameters and "–broad –qvalue 0.01", followed by filtering against very small (<20bp) or large (>10kb) peaks and against overlap with problematic regions of the genome[65]. Differential peak counts were computed using DiffBind[86] with default settings.

**Single-cell proteomics**

Single-cell samples were prepared using the droplet nPOP method as detailed in[42]. Sets of 14 single cells were run with a carrier sample of 100 cells of bulk digest labeled with TMT 126C and a 5-cell reference labeled with TMT 127N prepared via mPOP sample preparation[87,88]. Channels 127C and 128N were not used due to isotopic contaminants from the carrier channel.

For LC/MS analysis, samples were separated via online nLC on a Dionex UltiMate 3000 UHPLC; 1 µl out of 1.1 µl of sample was loaded onto a 25 cm × 75 1 µm IonOpticks Aurora Series UHPLC column (AUR2-25075C18A). Buffer A was 0.1% formic acid in water and buffer B was 0.1% formic acid in 80% acetonitrile / 20% water. Samples were analyzed by a Q-Exactive mass spectrometer (Thermo Scientific). After a precursor scan from 450 to 1600 m/z at 70,000 resolving power, the top 7 most intense precursor ions were isolated for MS2 analysis via a 0.7 Th isolation window with a 0.3 Th offset. These ions were accumulated for at most 500 ms before being fragmented via HCD at a normalized collision energy of 33 eV (normalized to m/z 500, z = 1). The fragments were analyzed at 140,000 resolving power.

Single cell MS data was preprocessed via the SCoPE2 data pipeline[89,90]. Cell types were then assigned via label transfer performed with LIGER[91]. Statistical tests between genotypes were performed via a t-test comparing protein expression between groups of single cells, using the Benjamini-Hochberg adjustment to correct for multiple hypotheses testing. Data and code are reported in accordance with community guidelines[92] and are available on github (https://github.com/SlavovLab/SC_Pancreas_KO).

**Ligand-receptor interaction analysis**

Single-cell RNA-sequencing data was analyzed using CellChat[93] (v.2.1.2) to infer intercellular communication changes in *Dec1-βKO* vs. wild-type islets. Enriched signaling genes and ligand-receptor interactions in each genotype were identified using the "identifyOverExpressedGenes" and "identifyOverExpressedInteractions" functions with default settings. A protein-protein interaction network was applied to smooth predictions. Communication probabilities were computed with "computeCommunProb" and filtered to exclude interactions involving <10 cells. Pathway-level predictions were refined using "computeCommunProbPathway", and communication networks were aggregated with "aggregateNet". Network centrality was assessed via "netAnalysis_computeCentrality", highlighting key signaling roles such as influencers or receivers within each genotype. To identify the top 10 differentially active pathways ($p < 0.01$ for change in communication probability between *Dec1-βKO* and wild-type), the overall information flow through signaling pathways across all cell types was ranked using the "rankNet" function. We then selected ligand-receptor pairs where the ligand is significantly altered ($p < 0.05$) in β1 cells (β cells with higher expression of insulin and maturity markers) and calculated the log2 fold

change in communication strength between *Dec1-βKO* vs. wild-type cells to quantify the change in communication flow.

**Cellular and mitochondrial energetics**

Live-cell imaging of stained mitochondria was conducted in mouse islets after an overnight recovery from isolation. All incubations were performed at 37°C with 5% $CO_2$. 30 islets were hand-picked, dissociated using TrypLE Express (Life Technologies), and the single cells seeded onto glass-bottom dishes (Cellvis; D29-14-1.5-N) pre-coated with 500ng/ml concanavalin A (Sigma; C2010) and incubated for 30 minutes to facilitate attachment. For mitochondrial staining, plated cells were incubated with freshly prepared 30nM MitoTracker Red CMXRos (Invitrogen; V35116) in RPMI-1640 medium (Life Technologies; 11875-093) for 30 minutes, followed by washing three times and replenishing with pre-warmed RPMI-1640 medium. Z-stack images were acquired with a Leica Stellaris 5 Confocal microscope and pre-processed by deconvolution using the PSF generator and DeconvolutionLab2 plugins in FIJI[94]. The Mitochondria Analyzer tool[95] was then used to skeletonize the deconvoluted z-stack images and quantify morphometric parameters.

Flow cytometry analysis of mitochondrial content, activity, cellular ROS, and glucose uptake was conducted in mouse islets dissociated as above. Single cell preparations were stained with freshly prepared solutions of either MitoTracker Green FM (Invitrogen; M46750; 1:2000) and 5µM CellROX Deep Red (Invitrogen; C10422), 50nM TMRE (Abcam; ab113852), or 20uM 2-NBDG (Invitrogen; N13195) in RMPI-1640 medium and incubated for 30 minutes at 37°C with 5% $CO_2$. Samples were then washed twice with 1% BSA in 1x PBS and filtered through a

40µm nylon mesh into flow cytometry tubes (STELLAR SCIENTIFIC; FSC-9005). Flow cytometry was conducted with a BD Accuri C6 Plus flow cytometer and analyzed using FlowJo v10.8.1 (BD Life Sciences).

**Metabolic flux analysis**

The Agilent Seahorse XFe96 Spheroid FluxPak (Agilent; 102905-100) and Seahorse XFe96 Analyzer were used to measure the oxygen consumption rate (OCR) and extracellular acidification rate (ECAR) of mouse islets after an overnight recovery from isolation. Subsequent incubations were performed in a 37°C $CO_2$-free incubator. The day before the experiment, sensor cartridge wells were rehydrated by incubating with 200µL of Agilent calibrant overnight, and the experimental wells of the spheroid plate were pre-coated with 30µL of 100 ng/mL poly-D-lysine (Sigma; P7280). Injection basal media (Agilent; 103335-100), wash media (basal media with 0.5% FBS), and assay media (basal media with 0.5% FBS and 1mM glucose) were freshly prepared and stored at 4°C protected from light. On the day of the experiment, all media were adjusted to pH 7.4 and warmed and kept at 37°C. Islets were hand-picked, incubated in wash media for two sequential 15-minute washes at room temperature, and transferred to each well of the spheroid plate pre-loaded with 175µL of assay medium (12 islets in a 30µL volume per well) using an islet-loading mold by gravity. The spheroid plate with loaded islets was then equilibrated for 1hr at 37°C. The Seahorse XFe96 Analyzer was calibrated with the cartridge plate for 15 minutes before data acquisition. The following compounds were then freshly prepared in 20µL of injection media and sequentially added by automatic pneumatic injection to reach final concentrations (after injection) of 16.7mM glucose with 0.5mM glutamine and 3.5mM amino acid mix; 5µM Oligomycin (Sigma; O4876); 2µM FCCP (Sigma; C2920); and

5µM Rotenone (Sigma; 557368) with 5µM Antimycin A (Sigma; A8674). Samples were subjected to the following numbers of assay cycles: 6 for basal OCR measurement; 4 for 16.7mM glucose + amino acids; 5 for Oligomycin; 4 for FCCP; and 6 for Rotenone + Antimycin A, with each cycle comprising 2 minutes of mixing and 3 minutes of OCR measurement. To normalize data by islet equivalents (IEQ), images of each experimental well were captured using a Cytation 5 instrument (Agilent) at the end of the experiment.

**Calcium influx**

Extracellular calcium influx dynamics were assayed in mouse islets after an overnight recovery from isolation as previously described[96]. Islets were washed two times with Krebs buffer, followed by staining with 16.7µM Fura2-AM (Life Technologies; F- F1225) in Krebs buffer supplemented with 5mM glucose for 45 minutes at 37°C. Islets were then transferred to a perifusion chamber on a homeothermic platform, perifused with 37°C Krebs buffer at a flow rate of 1mL/min. and imaged with an inverted Zeiss microscope (Axio Observer.Z1). After imaging in the absence of substrate, a physiological amino acids mixture (0.5 mM glutamine and 3.5mM amino acid mix) alone and with increasing glucose levels (3mM, 16.7mM) were sequentially applied, followed by washing all substrates away and applying KCl (30mM). Intracellular $Ca^{2+}$ was measured by dual-wavelength fluorescence microscopy using the Zeiss AxioVision system as previously described[97].

**Rigor and reproducibility**

Mice from at least two independent littermate cohorts for each genotype were assayed for each experiment. All mice were housed individually for metabolic assays, with at least 1 week to recover between assays, including light/dark-phase measurements for the same cohort. Mice of all genotypes were assayed in parallel, blinded for genotype whenever possible, to minimize ascertainment bias. Differential gene regulation was validated across genomic/proteomic assays performed on independent mouse cohorts.

## QUANTIFICATION AND STATISTICAL ANALYSIS

No statistical methods were used to predetermine sample size or remove outliers. To assess the statistical difference between two sets of unpaired data, a Shapiro-Wilk normality test was first performed via the shapiro.test R implementation with default parameters. Normally distributed data was then tested for equality of variance using the Bartlett.test R implementation with default parameters. A two-sided t-test (t.test R implementation with default parameters and var.equal =FALSE or TRUE) was then used to assess confidence on the measured difference of their mean values. For unpaired data that did not follow a normal distribution, we used a non-parametric Wilcoxon rank sum test to determine if they belong to the same parent distribution.

## DATA AND CODE AVAILABILITY

Raw and processed sequencing data generated in this study are available at NCBI GEO accession number GSE289105. Proteomic raw data are deposited at MassIVE (MSV000092610). Processed proteomic data can be accessed at https://shorturl.at/DNWY8.

## EXCEL TABLE TITLE AND LEGENDS

**Table S1. DEC1, DEC2, BMAL1, CLOCK, and PDX1 ChIP-sequencing peaks union.**

**Table S2. Genes bound by DEC1 and differentially rhythmic/expressed in Dec1-βKO islets.**

**Table S3. Gene ontology enrichment analysis of DEC1-bound genes differentially rhythmic and differentially expressed in Dec1-βKO islets.**

**Table S4. Datasets used in this study.**

## REFERENCES


1. Bass, J., and Lazar, M.A. (2016). Circadian time signatures of fitness and disease. Science *354*, 994-999. 10.1126/science.aah4965.
2. Panda, S. (2016). Circadian physiology of metabolism. Science *354*, 1008-1015. 10.1126/science.aah4967.
3. Panda, S., Hogenesch, J.B., and Kay, S.A. (2002). Circadian rhythms from flies to human. Nature *417*, 329-335. 10.1038/417329a.
4. Takahashi, J.S. (2017). Transcriptional architecture of the mammalian circadian clock. Nat Rev Genet *18*, 164-179. 10.1038/nrg.2016.150.
5. Bass, J., and Takahashi, J.S. (2010). Circadian integration of metabolism and energetics. Science *330*, 1349-1354. 10.1126/science.1195027.
6. Koronowski, K.B., and Sassone-Corsi, P. (2021). Communicating clocks shape circadian homeostasis. Science *371*. 10.1126/science.abd0951.
7. Umemura, Y., and Yagita, K. (2020). Development of the Circadian Core Machinery in Mammals. J Mol Biol *432*, 3611-3617. 10.1016/j.jmb.2019.11.026.
8. Dierickx, P., Van Laake, L.W., and Geijsen, N. (2018). Circadian clocks: from stem cells to tissue homeostasis and regeneration. EMBO Rep *19*, 18-28. 10.15252/embr.201745130.
9. Alvarez-Dominguez, J.R., and Melton, D.A. (2022). Cell maturation: Hallmarks, triggers, and manipulation. Cell *185*, 235-249. 10.1016/j.cell.2021.12.012.
10. Du Pre, B.C., Van Veen, T.A., Young, M.E., Vos, M.A., Doevendans, P.A., and Van Laake, L.W. (2014). Circadian rhythms in cell maturation. Physiology (Bethesda) *29*, 72-83. 10.1152/physiol.00036.2013.

11. Zhang, E.E., and Kay, S.A. (2010). Clocks not winding down: unravelling circadian networks. Nat Rev Mol Cell Biol *11*, 764-776. 10.1038/nrm2995.
12. Guan, D., and Lazar, M.A. (2021). Interconnections between circadian clocks and metabolism. J Clin Invest *131*. 10.1172/JCI148278.
13. Turek, F.W., Joshu, C., Kohsaka, A., Lin, E., Ivanova, G., McDearmon, E., Laposky, A., Losee-Olson, S., Easton, A., Jensen, D.R., et al. (2005). Obesity and metabolic syndrome in circadian Clock mutant mice. Science *308*, 1043-1045. 10.1126/science.1108750.
14. Rudic, R.D., McNamara, P., Curtis, A.M., Boston, R.C., Panda, S., Hogenesch, J.B., and Fitzgerald, G.A. (2004). BMAL1 and CLOCK, two essential components of the circadian clock, are involved in glucose homeostasis. PLoS Biol *2*, e377. 10.1371/journal.pbio.0020377.
15. Marcheva, B., Ramsey, K.M., Buhr, E.D., Kobayashi, Y., Su, H., Ko, C.H., Ivanova, G., Omura, C., Mo, S., Vitaterna, M.H., et al. (2010). Disruption of the clock components CLOCK and BMAL1 leads to hypoinsulinaemia and diabetes. Nature *466*, 627-631. 10.1038/nature09253.
16. Gao, Y., Gan, T., Jiang, L., Yu, L., Tang, D., Wang, Y., Li, X., and Ding, G. (2020). Association between shift work and risk of type 2 diabetes mellitus: a systematic review and dose-response meta-analysis of observational studies. Chronobiol Int *37*, 29-46. 10.1080/07420528.2019.1683570.
17. Scheer, F.A., Hilton, M.F., Mantzoros, C.S., and Shea, S.A. (2009). Adverse metabolic and cardiovascular consequences of circadian misalignment. Proc Natl Acad Sci U S A *106*, 4453-4458. 10.1073/pnas.0808180106.
18. Schrader, L.A., Ronnekleiv-Kelly, S.M., Hogenesch, J.B., Bradfield, C.A., and Malecki, K.M. (2024). Circadian disruption, clock genes, and metabolic health. J Clin Invest *134*. 10.1172/JCI170998.
19. Van Cauter, E., Polonsky, K.S., and Scheen, A.J. (1997). Roles of circadian rhythmicity and sleep in human glucose regulation. Endocr Rev *18*, 716-738. 10.1210/edrv.18.5.0317.
20. Perelis, M., Ramsey, K.M., Marcheva, B., and Bass, J. (2016). Circadian Transcription from Beta Cell Function to Diabetes Pathophysiology. J Biol Rhythms *31*, 323-336. 10.1177/0748730416656949.
21. Sadacca, L.A., Lamia, K.A., deLemos, A.S., Blum, B., and Weitz, C.J. (2011). An intrinsic circadian clock of the pancreas is required for normal insulin release and glucose homeostasis in mice. Diabetologia *54*, 120-124. 10.1007/s00125-010-1920-8.
22. Lee, J., Kim, M.S., Li, R., Liu, V.Y., Fu, L., Moore, D.D., Ma, K., and Yechoor, V.K. (2011). Loss of Bmal1 leads to uncoupling and impaired glucose-stimulated insulin secretion in beta-cells. Islets *3*, 381-388. 10.4161/isl.3.6.18157.
23. Perelis, M., Marcheva, B., Ramsey, K.M., Schipma, M.J., Hutchison, A.L., Taguchi, A., Peek, C.B., Hong, H., Huang, W., Omura, C., et al. (2015). Pancreatic beta cell enhancers regulate rhythmic transcription of genes controlling insulin secretion. Science *350*, aac4250. 10.1126/science.aac4250.
24. Alvarez-Dominguez, J.R., Donaghey, J., Rasouli, N., Kenty, J.H.R., Helman, A., Charlton, J., Straubhaar, J.R., Meissner, A., and Melton, D.A. (2020). Circadian Entrainment Triggers Maturation of Human In Vitro Islets. Cell Stem Cell *26*, 108-122 e110. 10.1016/j.stem.2019.11.011.
25. Hang, Y., Yamamoto, T., Benninger, R.K., Brissova, M., Guo, M., Bush, W., Piston, D.W., Powers, A.C., Magnuson, M., Thurmond, D.C., and Stein, R. (2014). The MafA transcription factor becomes essential to islet beta-cells soon after birth. Diabetes *63*, 1994-2005. 10.2337/db13-1001.
26. Aguayo-Mazzucato, C., Koh, A., El Khattabi, I., Li, W.C., Toschi, E., Jermendy, A., Juhl, K., Mao, K., Weir, G.C., Sharma, A., and Bonner-Weir, S. (2011). Mafa expression enhances glucose-

responsive insulin secretion in neonatal rat beta cells. Diabetologia *54*, 583-593. 10.1007/s00125-010-2026-z.

27. Kato, Y., Kawamoto, T., Fujimoto, K., and Noshiro, M. (2014). DEC1/STRA13/SHARP2 and DEC2/SHARP1 coordinate physiological processes, including circadian rhythms in response to environmental stimuli. Curr Top Dev Biol *110*, 339-372. 10.1016/B978-0-12-405943-6.00010-5.
28. Honma, S., Kawamoto, T., Takagi, Y., Fujimoto, K., Sato, F., Noshiro, M., Kato, Y., and Honma, K. (2002). Dec1 and Dec2 are regulators of the mammalian molecular clock. Nature *419*, 841-844. 10.1038/nature01123.
29. Jiang, X., Tian, F., Du, Y., Copeland, N.G., Jenkins, N.A., Tessarollo, L., Wu, X., Pan, H., Hu, X.Z., Xu, K., et al. (2008). BHLHB2 controls Bdnf promoter 4 activity and neuronal excitability. J Neurosci *28*, 1118-1130. 10.1523/JNEUROSCI.2262-07.2008.
30. Rossner, M.J., Oster, H., Wichert, S.P., Reinecke, L., Wehr, M.C., Reinecke, J., Eichele, G., Taneja, R., and Nave, K.A. (2008). Disturbed clockwork resetting in Sharp-1 and Sharp-2 single and double mutant mice. PLoS One *3*, e2762. 10.1371/journal.pone.0002762.
31. Nakashima, A., Kawamoto, T., Honda, K.K., Ueshima, T., Noshiro, M., Iwata, T., Fujimoto, K., Kubo, H., Honma, S., Yorioka, N., et al. (2008). DEC1 modulates the circadian phase of clock gene expression. Mol Cell Biol *28*, 4080-4092. 10.1128/MCB.02168-07.
32. Gu, C., Stein, G.H., Pan, N., Goebbels, S., Hornberg, H., Nave, K.A., Herrera, P., White, P., Kaestner, K.H., Sussel, L., and Lee, J.E. (2010). Pancreatic beta cells require NeuroD to achieve and maintain functional maturity. Cell Metab *11*, 298-310. 10.1016/j.cmet.2010.03.006.
33. Guillam, M.T., Hummler, E., Schaerer, E., Yeh, J.I., Birnbaum, M.J., Beermann, F., Schmidt, A., Deriaz, N., and Thorens, B. (1997). Early diabetes and abnormal postnatal pancreatic islet development in mice lacking Glut-2. Nat Genet *17*, 327-330. 10.1038/ng1197-327.
34. Metukuri, M.R., Zhang, P., Basantani, M.K., Chin, C., Stamateris, R.E., Alonso, L.C., Takane, K.K., Gramignoli, R., Strom, S.C., O'Doherty, R.M., et al. (2012). ChREBP mediates glucose-stimulated pancreatic beta-cell proliferation. Diabetes *61*, 2004-2015. 10.2337/db11-0802.
35. Weger, B.D., Gobet, C., David, F.P.A., Atger, F., Martin, E., Phillips, N.E., Charpagne, A., Weger, M., Naef, F., and Gachon, F. (2021). Systematic analysis of differential rhythmic liver gene expression mediated by the circadian clock and feeding rhythms. Proc Natl Acad Sci U S A *118*. 10.1073/pnas.2015803118.
36. Saini, C., Petrenko, V., Pulimeno, P., Giovannoni, L., Berney, T., Hebrok, M., Howald, C., Dermitzakis, E.T., and Dibner, C. (2016). A functional circadian clock is required for proper insulin secretion by human pancreatic islet cells. Diabetes Obes Metab *18*, 355-365. 10.1111/dom.12616.
37. Blum, B., Hrvatin, S., Schuetz, C., Bonal, C., Rezania, A., and Melton, D.A. (2012). Functional beta-cell maturation is marked by an increased glucose threshold and by expression of urocortin 3. Nat Biotechnol *30*, 261-264. 10.1038/nbt.2141.
38. Aguayo-Mazzucato, C., Sanchez-Soto, C., Godinez-Puig, V., Gutierrez-Ospina, G., and Hiriart, M. (2006). Restructuring of pancreatic islets and insulin secretion in a postnatal critical window. PLoS One *1*, e35. 10.1371/journal.pone.0000035.
39. Walker, J.T., Saunders, D.C., Brissova, M., and Powers, A.C. (2021). The Human Islet: Mini-Organ With Mega-Impact. Endocr Rev *42*, 605-657. 10.1210/endrev/bnab010.
40. Noguchi, G.M., and Huising, M.O. (2019). Integrating the inputs that shape pancreatic islet hormone release. Nat Metab *1*, 1189-1201. 10.1038/s42255-019-0148-2.
41. Budnik, B., Levy, E., Harmange, G., and Slavov, N. (2018). SCoPE-MS: mass spectrometry of single mammalian cells quantifies proteome heterogeneity during cell differentiation. Genome Biol *19*, 161. 10.1186/s13059-018-1547-5.

42. Leduc, A., Huffman, R.G., Cantlon, J., Khan, S., and Slavov, N. (2022). Exploring functional protein covariation across single cells using nPOP. Genome Biol *23*, 261. 10.1186/s13059-022-02817-5.
43. Stuart, T., Butler, A., Hoffman, P., Hafemeister, C., Papalexi, E., Mauck, W.M., 3rd, Hao, Y., Stoeckius, M., Smibert, P., and Satija, R. (2019). Comprehensive Integration of Single-Cell Data. Cell *177*, 1888-1902 e1821. 10.1016/j.cell.2019.05.031.
44. Veres, A., Faust, A.L., Bushnell, H.L., Engquist, E.N., Kenty, J.H., Harb, G., Poh, Y.C., Sintov, E., Gurtler, M., Pagliuca, F.W., et al. (2019). Charting cellular identity during human in vitro beta-cell differentiation. Nature *569*, 368-373. 10.1038/s41586-019-1168-5.
45. Katsumoto, K., Yennek, S., Chen, C., Silva, L.F.D., Traikov, S., Sever, D., Azad, A., Shan, J., Vainio, S., Ninov, N., et al. (2022). Wnt4 is heterogeneously activated in maturing beta-cells to control calcium signaling, metabolism and function. Nat Commun *13*, 6255. 10.1038/s41467-022-33841-5.
46. Yang, J., Hammoud, B., Ridler, A., Won, K.-J., Hoshi, T., Stanley, C.A., Stanescu, D.E., and Ackermann, A.M. (2021). Early postnatal activation of the hypoxia pathway disrupts β-cell function. bioRxiv, 2021.2006.2009.447705. 10.1101/2021.06.09.447705.
47. Monteiro, P., Rosse, C., Castro-Castro, A., Irondelle, M., Lagoutte, E., Paul-Gilloteaux, P., Desnos, C., Formstecher, E., Darchen, F., Perrais, D., et al. (2013). Endosomal WASH and exocyst complexes control exocytosis of MT1-MMP at invadopodia. J Cell Biol *203*, 1063-1079. 10.1083/jcb.201306162.
48. Peschke, E., and Peschke, D. (1998). Evidence for a circadian rhythm of insulin release from perifused rat pancreatic islets. Diabetologia *41*, 1085-1092. 10.1007/s001250051034.
49. Schmitt, K., Grimm, A., Dallmann, R., Oettinghaus, B., Restelli, L.M., Witzig, M., Ishihara, N., Mihara, K., Ripperger, J.A., Albrecht, U., et al. (2018). Circadian Control of DRP1 Activity Regulates Mitochondrial Dynamics and Bioenergetics. Cell Metab *27*, 657-666 e655. 10.1016/j.cmet.2018.01.011.
50. Beytebiere, J.R., Greenwell, B.J., Sahasrabudhe, A., and Menet, J.S. (2019). Clock-controlled rhythmic transcription: is the clock enough and how does it work? Transcription *10*, 212-221. 10.1080/21541264.2019.1673636.
51. Liu, A.C., Tran, H.G., Zhang, E.E., Priest, A.A., Welsh, D.K., and Kay, S.A. (2008). Redundant function of REV-ERBalpha and beta and non-essential role for Bmal1 cycling in transcriptional regulation of intracellular circadian rhythms. PLoS Genet *4*, e1000023. 10.1371/journal.pgen.1000023.
52. Kim, Y.H., and Lazar, M.A. (2020). Transcriptional Control of Circadian Rhythms and Metabolism: A Matter of Time and Space. Endocr Rev *41*, 707-732. 10.1210/endrev/bnaa014.
53. Kreslavsky, T., Vilagos, B., Tagoh, H., Poliakova, D.K., Schwickert, T.A., Wohner, M., Jaritz, M., Weiss, S., Taneja, R., Rossner, M.J., and Busslinger, M. (2017). Essential role for the transcription factor Bhlhe41 in regulating the development, self-renewal and BCR repertoire of B-1a cells. Nat Immunol *18*, 442-455. 10.1038/ni.3694.
54. Consortium, E.P. (2012). An integrated encyclopedia of DNA elements in the human genome. Nature *489*, 57-74. 10.1038/nature11247.
55. Rakshit, K., Hsu, T.W., and Matveyenko, A.V. (2016). Bmal1 is required for beta cell compensatory expansion, survival and metabolic adaptation to diet-induced obesity in mice. Diabetologia *59*, 734-743. 10.1007/s00125-015-3859-2.
56. Bideyan, L., Nagari, R., and Tontonoz, P. (2021). Hepatic transcriptional responses to fasting and feeding. Genes Dev *35*, 635-657. 10.1101/gad.348340.121.
57. Rakshit, K., Qian, J., Gaonkar, K.S., Dhawan, S., Colwell, C.S., and Matveyenko, A.V. (2018). Postnatal Ontogenesis of the Islet Circadian Clock Plays a Contributory Role in beta-Cell Maturation Process. Diabetes *67*, 911-922. 10.2337/db17-0850.

58. Hogrebe, N.J., Ishahak, M., and Millman, J.R. (2023). Developments in stem cell-derived islet replacement therapy for treating type 1 diabetes. Cell Stem Cell *30*, 530-548. 10.1016/j.stem.2023.04.002.
59. Leavens, K.F., Alvarez-Dominguez, J.R., Vo, L.T., Russ, H.A., and Parent, A.V. (2022). Stem cell-based multi-tissue platforms to model human autoimmune diabetes. Mol Metab *66*, 101610. 10.1016/j.molmet.2022.101610.
60. Postic, C., Shiota, M., Niswender, K.D., Jetton, T.L., Chen, Y., Moates, J.M., Shelton, K.D., Lindner, J., Cherrington, A.D., and Magnuson, M.A. (1999). Dual roles for glucokinase in glucose homeostasis as determined by liver and pancreatic beta cell-specific gene knock-outs using Cre recombinase. J Biol Chem *274*, 305-315. 10.1074/jbc.274.1.305.
61. Mina, A.I., LeClair, R.A., LeClair, K.B., Cohen, D.E., Lantier, L., and Banks, A.S. (2018). CalR: A Web-Based Analysis Tool for Indirect Calorimetry Experiments. Cell Metab *28*, 656-666 e651. 10.1016/j.cmet.2018.06.019.
62. Li, D.S., Yuan, Y.H., Tu, H.J., Liang, Q.L., and Dai, L.J. (2009). A protocol for islet isolation from mouse pancreas. Nat Protoc *4*, 1649-1652. 10.1038/nprot.2009.150.
63. Dobin, A., Davis, C.A., Schlesinger, F., Drenkow, J., Zaleski, C., Jha, S., Batut, P., Chaisson, M., and Gingeras, T.R. (2013). STAR: ultrafast universal RNA-seq aligner. Bioinformatics *29*, 15-21. 10.1093/bioinformatics/bts635.
64. Zhang, Y., Liu, T., Meyer, C.A., Eeckhoute, J., Johnson, D.S., Bernstein, B.E., Nusbaum, C., Myers, R.M., Brown, M., Li, W., and Liu, X.S. (2008). Model-based analysis of ChIP-Seq (MACS). Genome Biol *9*, R137. 10.1186/gb-2008-9-9-r137.
65. Amemiya, H.M., Kundaje, A., and Boyle, A.P. (2019). The ENCODE Blacklist: Identification of Problematic Regions of the Genome. Sci Rep *9*, 9354. 10.1038/s41598-019-45839-z.
66. Quinlan, A.R., and Hall, I.M. (2010). BEDTools: a flexible suite of utilities for comparing genomic features. Bioinformatics *26*, 841-842. 10.1093/bioinformatics/btq033.
67. Anders, S., Pyl, P.T., and Huber, W. (2015). HTSeq--a Python framework to work with high-throughput sequencing data. Bioinformatics *31*, 166-169. 10.1093/bioinformatics/btu638.
68. Newburger, D.E., and Bulyk, M.L. (2009). UniPROBE: an online database of protein binding microarray data on protein-DNA interactions. Nucleic Acids Res *37*, D77-82. 10.1093/nar/gkn660.
69. Sandelin, A., Alkema, W., Engstrom, P., Wasserman, W.W., and Lenhard, B. (2004). JASPAR: an open-access database for eukaryotic transcription factor binding profiles. Nucleic Acids Res *32*, D91-94. 10.1093/nar/gkh012.
70. Jolma, A., Yan, J., Whitington, T., Toivonen, J., Nitta, K.R., Rastas, P., Morgunova, E., Enge, M., Taipale, M., Wei, G., et al. (2013). DNA-binding specificities of human transcription factors. Cell *152*, 327-339. 10.1016/j.cell.2012.12.009.
71. Machanick, P., and Bailey, T.L. (2011). MEME-ChIP: motif analysis of large DNA datasets. Bioinformatics *27*, 1696-1697. 10.1093/bioinformatics/btr189.
72. Bailey, T.L., and Machanick, P. (2012). Inferring direct DNA binding from ChIP-seq. Nucleic Acids Res *40*, e128. 10.1093/nar/gks433.
73. Gupta, S., Stamatoyannopoulos, J.A., Bailey, T.L., and Noble, W.S. (2007). Quantifying similarity between motifs. Genome Biol *8*, R24. 10.1186/gb-2007-8-2-r24.
74. Grant, C.E., Bailey, T.L., and Noble, W.S. (2011). FIMO: scanning for occurrences of a given motif. Bioinformatics *27*, 1017-1018. 10.1093/bioinformatics/btr064.
75. Zhou, Y., Zhou, B., Pache, L., Chang, M., Khodabakhshi, A.H., Tanaseichuk, O., Benner, C., and Chanda, S.K. (2019). Metascape provides a biologist-oriented resource for the analysis of systems-level datasets. Nat Commun *10*, 1523. 10.1038/s41467-019-09234-6.

76. Heinz, S., Benner, C., Spann, N., Bertolino, E., Lin, Y.C., Laslo, P., Cheng, J.X., Murre, C., Singh, H., and Glass, C.K. (2010). Simple combinations of lineage-determining transcription factors prime cis-regulatory elements required for macrophage and B cell identities. Mol Cell *38*, 576-589. 10.1016/j.molcel.2010.05.004.
77. Anders, S., and Huber, W. (2010). Differential expression analysis for sequence count data. Genome Biol *11*, R106. 10.1186/gb-2010-11-10-r106.
78. Zhang, R., Podtelezhnikov, A.A., Hogenesch, J.B., and Anafi, R.C. (2016). Discovering Biology in Periodic Data through Phase Set Enrichment Analysis (PSEA). J Biol Rhythms *31*, 244-257. 10.1177/0748730416631895.
79. Thaben, P.F., and Westermark, P.O. (2014). Detecting rhythms in time series with RAIN. J Biol Rhythms *29*, 391-400. 10.1177/0748730414553029.
80. Helman, A., Cangelosi, A.L., Davis, J.C., Pham, Q., Rothman, A., Faust, A.L., Straubhaar, J.R., Sabatini, D.M., and Melton, D.A. (2020). A Nutrient-Sensing Transition at Birth Triggers Glucose-Responsive Insulin Secretion. Cell Metab *31*, 1004-1016 e1005. 10.1016/j.cmet.2020.04.004.
81. Luecken, M.D., and Theis, F.J. (2019). Current best practices in single-cell RNA-seq analysis: a tutorial. Mol Syst Biol *15*, e8746. 10.15252/msb.20188746.
82. Chiou, J., Zeng, C., Cheng, Z., Han, J.Y., Schlichting, M., Miller, M., Mendez, R., Huang, S., Wang, J., Sui, Y., et al. (2021). Single-cell chromatin accessibility identifies pancreatic islet cell type- and state-specific regulatory programs of diabetes risk. Nat Genet *53*, 455-466. 10.1038/s41588-021-00823-0.
83. Li, B., and Dewey, C.N. (2011). RSEM: accurate transcript quantification from RNA-Seq data with or without a reference genome. BMC Bioinformatics *12*, 323. 10.1186/1471-2105-12-323.
84. Sharon, N., Chawla, R., Mueller, J., Vanderhooft, J., Whitehorn, L.J., Rosenthal, B., Gurtler, M., Estanboulieh, R.R., Shvartsman, D., Gifford, D.K., et al. (2019). A Peninsular Structure Coordinates Asynchronous Differentiation with Morphogenesis to Generate Pancreatic Islets. Cell *176*, 790-804 e713. 10.1016/j.cell.2018.12.003.
85. Robinson, M.D., McCarthy, D.J., and Smyth, G.K. (2010). edgeR: a Bioconductor package for differential expression analysis of digital gene expression data. Bioinformatics *26*, 139-140. 10.1093/bioinformatics/btp616.
86. Ross-Innes, C.S., Stark, R., Teschendorff, A.E., Holmes, K.A., Ali, H.R., Dunning, M.J., Brown, G.D., Gojis, O., Ellis, I.O., Green, A.R., et al. (2012). Differential oestrogen receptor binding is associated with clinical outcome in breast cancer. Nature *481*, 389-393. 10.1038/nature10730.
87. Specht, H., Harmange, G., Perlman, D.H., Emmott, E., Niziolek, Z., Budnik, B., and Slavov, N. (2018). Automated sample preparation for high-throughput single-cell proteomics. bioRxiv, 399774. 10.1101/399774.
88. Petelski, A.A., Emmott, E., Leduc, A., Huffman, R.G., Specht, H., Perlman, D.H., and Slavov, N. (2021). Multiplexed single-cell proteomics using SCoPE2. Nat Protoc *16*, 5398-5425. 10.1038/s41596-021-00616-z.
89. Specht, H., Emmott, E., Petelski, A.A., Huffman, R.G., Perlman, D.H., Serra, M., Kharchenko, P., Koller, A., and Slavov, N. (2021). Single-cell proteomic and transcriptomic analysis of macrophage heterogeneity using SCoPE2. Genome Biol *22*, 50. 10.1186/s13059-021-02267-5.
90. Specht, H., and Slavov, N. (2021). Optimizing Accuracy and Depth of Protein Quantification in Experiments Using Isobaric Carriers. J Proteome Res *20*, 880-887. 10.1021/acs.jproteome.0c00675.
91. Liu, J., Gao, C., Sodicoff, J., Kozareva, V., Macosko, E.Z., and Welch, J.D. (2020). Jointly defining cell types from multiple single-cell datasets using LIGER. Nat Protoc *15*, 3632-3662. 10.1038/s41596-020-0391-8.

92. Gatto, L., Aebersold, R., Cox, J., Demichev, V., Derks, J., Emmott, E., Franks, A.M., Ivanov, A.R., Kelly, R.T., Khoury, L., et al. (2023). Initial recommendations for performing, benchmarking and reporting single-cell proteomics experiments. Nat Methods *20*, 375-386. 10.1038/s41592-023-01785-3.
93. Jin, S., Guerrero-Juarez, C.F., Zhang, L., Chang, I., Ramos, R., Kuan, C.H., Myung, P., Plikus, M.V., and Nie, Q. (2021). Inference and analysis of cell-cell communication using CellChat. Nat Commun *12*, 1088. 10.1038/s41467-021-21246-9.
94. Schindelin, J., Arganda-Carreras, I., Frise, E., Kaynig, V., Longair, M., Pietzsch, T., Preibisch, S., Rueden, C., Saalfeld, S., Schmid, B., et al. (2012). Fiji: an open-source platform for biological-image analysis. Nat Methods *9*, 676-682. 10.1038/nmeth.2019.
95. Chaudhry, A., Shi, R., and Luciani, D.S. (2020). A pipeline for multidimensional confocal analysis of mitochondrial morphology, function, and dynamics in pancreatic beta-cells. Am J Physiol Endocrinol Metab *318*, E87-E101. 10.1152/ajpendo.00457.2019.
96. Kenty, J.H., and Melton, D.A. (2015). Testing pancreatic islet function at the single cell level by calcium influx with associated marker expression. PLoS One *10*, e0122044. 10.1371/journal.pone.0122044.
97. Doliba, N.M., Qin, W., Vinogradov, S.A., Wilson, D.F., and Matschinsky, F.M. (2010). Palmitic acid acutely inhibits acetylcholine- but not GLP-1-stimulated insulin secretion in mouse pancreatic islets. Am J Physiol Endocrinol Metab *299*, E475-485. 10.1152/ajpendo.00072.2010.

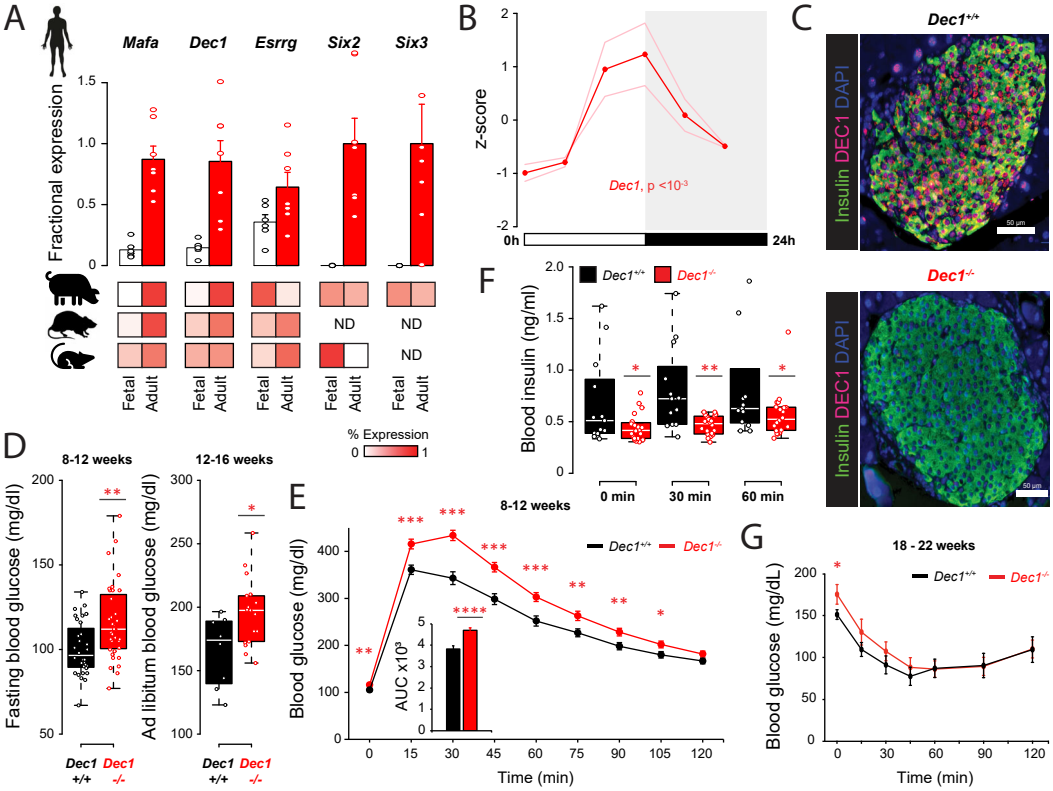
A
Mafa
Dec1
Esrrg
Six2
Six3
Fractional expression
ND
ND
ND
Fetal
Adult
% Expression
B
z-score
Dec1, p <10-3
0h
24h
C
Dec1+/+
Dec1-/-
Insulin DEC1 DAPI
F
Blood insulin (ng/ml)
0 min
30 min
60 min
D
8-12 weeks
12-16 weeks
Fasting blood glucose (mg/dl)
Ad libitum blood glucose (mg/dl)
Dec1 +/+
Dec1 -/-
E
8-12 weeks
Blood glucose (mg/dl)
AUC x10³
Time (min)
G
18 - 22 weeks
Blood glucose (mg/dL)
Time (min)

**Figure 1. DEC1 defines mature β cells and controls blood glucose homeostasis.**

(**A**) Specificity of *Dec1* transcription for adult β cells in N =2-3 humans, 2-11 pigs, 3 rats, and 1-3 mice, compared to adult-restricted transcription factors known to regulate human β-cell functional maturation. Data are mean ±SEM from unsynchronized β cells.

(**B**) *Dec1* oscillation in adult mouse β-cells isolated every 4h for a day. Data are mean of n =2 replicate measurements, each pooling N =6 mice. Rhythmicity p-value, RAIN.

(**C**) Immunofluorescence staining of insulin (green), DEC1 (red), and DAPI (blue) in *Dec1*$^{+/+}$ and *Dec1*$^{-/-}$ mice pancreata.

(**D**) Blood glucose in 14-hour fasted N =32 *Dec1*$^{+/+}$ and 36 *Dec1*$^{-/-}$ 2-3-month-old mice at ZT2 (left), and in *ad libitum* fed N =8 *Dec1*$^{+/+}$ and 17 *Dec1*$^{-/-}$ 3-4-month-old mice at ZT12 (right).

(**E**) Glucose tolerance in 14-hour fasted N =39 *Dec1*$^{+/+}$ and 42 *Dec1*$^{-/-}$ 2-3-month-old mice following intraperitoneal glucose administration at ZT2. Data are mean ±SEM.

(**F**) Blood insulin secretion in 14-hour fasted N =13 *Dec1*$^{+/+}$ and 20 *Dec1*$^{-/-}$ 8-month-old mice following intraperitoneal glucose administration at ZT2.

**(G)** Insulin tolerance of N =10 *Dec1*$^{+/+}$ and 7 *Dec1*$^{-/-}$ 4-5-month-old mice following intraperitoneal insulin administration at ZT2. Data are mean ±SEM.

*p <0.05, **p <1e-2, ***p <1e-3, ****p <1e-4, t test [(D), (E), (G)] and Wilcoxon test (F).

A

| Effect | Mass | *Dec1*$^{+/+}$ vs *Dec1*$^{-/-}$ | Interaction |
|---|---|---|---|
| Food consumed (kcal/period) | ** | 1.00 | |
| Water consumed (ml/period) | ** | 0.54 | |
| Energy expenditure (kcal/period) | ** | * | * |
| Oxygen consumption (ml/hr) | ** | * | * |
| Carbon dioxide production (ml/hr) | ** | * | * |
| Pedestrian locomotion (m) | | * | |
| Total distance in cage (m) | | * | |
| Respiratory exchange ratio | | 0.80 | |
| Locomotor activity (beam breaks) | | 0.53 | |
| Wheel running (counts) | | 0.17 | |
| Cumulative wheel running (counts) | | 0.34 | |

D

| Effect | Mass | *Dec1*$^{+/+}$ vs *Dec1*$^{-/-}$ | Interaction |
|---|---|---|---|
| Food consumed (kcal/period) | 0.11 | 0.78 | |
| Water consumed (ml/period) | 0.55 | 0.76 | |
| Energy expenditure (kcal/period) | ** | * | * |
| Oxygen consumption (ml/hr) | ** | * | * |
| Carbon dioxide production (ml/hr) | ** | * | * |
| Pedestrian locomotion (m) | | ** | |
| Total distance in cage (m) | | ** | |
| Respiratory exchange ratio | | 0.98 | |
| Locomotor activity (beam breaks) | | 0.43 | |
| Wheel running (counts) | | 0.38 | |
| Cumulative wheel running (counts) | | 0.72 | |

B

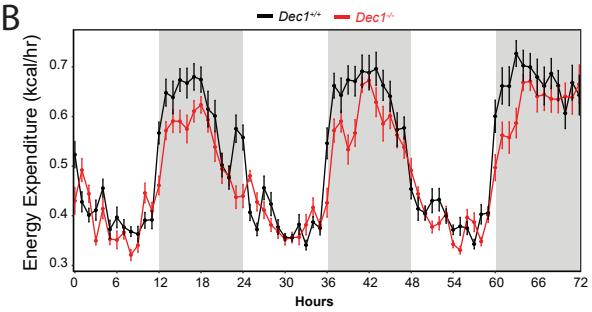


E

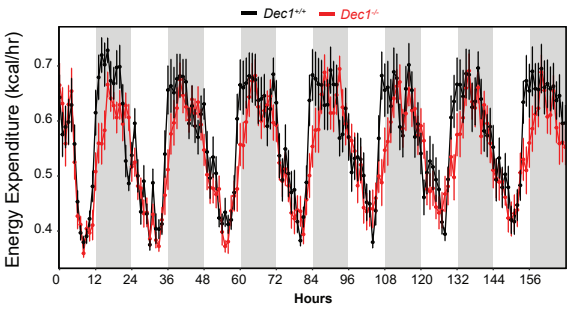


C

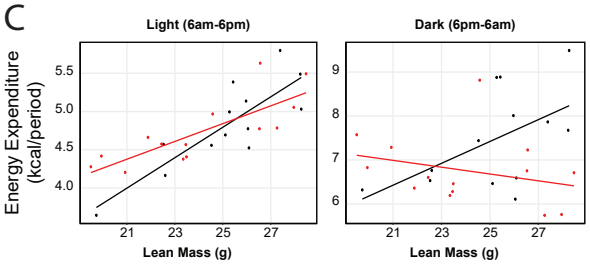


| Effect | Mass | Genotype | Interaction |
|---|---|---|---|
| p-value | *** | 0.58 | |

| Effect | Mass | Genotype | Interaction |
|---|---|---|---|
| p-value | * | * | * |

F

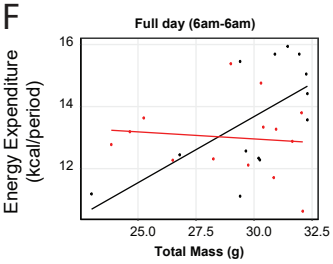


| Effect | Mass | Genotype | Interaction |
|---|---|---|---|
| p-value | ** | * | * |

G

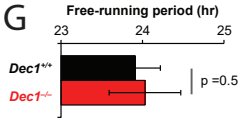


H

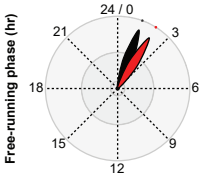

**Figure 2. DEC1 regulates circadian energy expenditure rhythms.**

(**A**) Summary of results from indirect calorimetry experiments for N =13 *Dec1*$^{+/+}$ and 14 *Dec1*$^{-/-}$ mice across 3 days in 12-hour light-dark cycles. Shown are p-values corresponding to model coefficients for genotype effects, along with the mass and interaction effects for mass-dependent measurements.

(**B**) Daily energy expenditure rhythms of N =13 *Dec1*$^{+/+}$ and 14 *Dec1*$^{-/-}$ mice across 3 days in 12-hour light-dark cycles. Data are mean ±SEM.

(**C**) Regression analysis of energy expenditure and body mass by photoperiod. Model coefficients for mass, genotype, and interaction effects are indicated below.

(**D**) Summary of results from indirect calorimetry experiments for N =13 *Dec1*$^{+/+}$ and 14 *Dec1*$^{-/-}$ mice across 7 days in 12-hour dark-dark cycles (constant darkness). Shown are p-values corresponding to model coefficients for genotype effects, along with the mass and interaction effects for mass-dependent measurements.

(**E**) Daily energy expenditure rhythms of N =13 *Dec1*$^{+/+}$ and 14 *Dec1*$^{-/-}$ mice across 7 days in 12-hour dark-dark cycles. Data are mean ±SEM.

(**F**) Regression analysis of energy expenditure as a function of body mass for the full circadian cycle. Model coefficients for mass, genotype, and interaction effects are indicated below.

(**G-H**) Free-running period (G) and phase (H) of wheel running rhythms of N =13 *Dec1*$^{+/+}$ and 14 *Dec1*$^{-/-}$ mice across 7 days in 12-hour dark-dark cycles.

*p <0.05, **p <0.01, ANCOVA test.

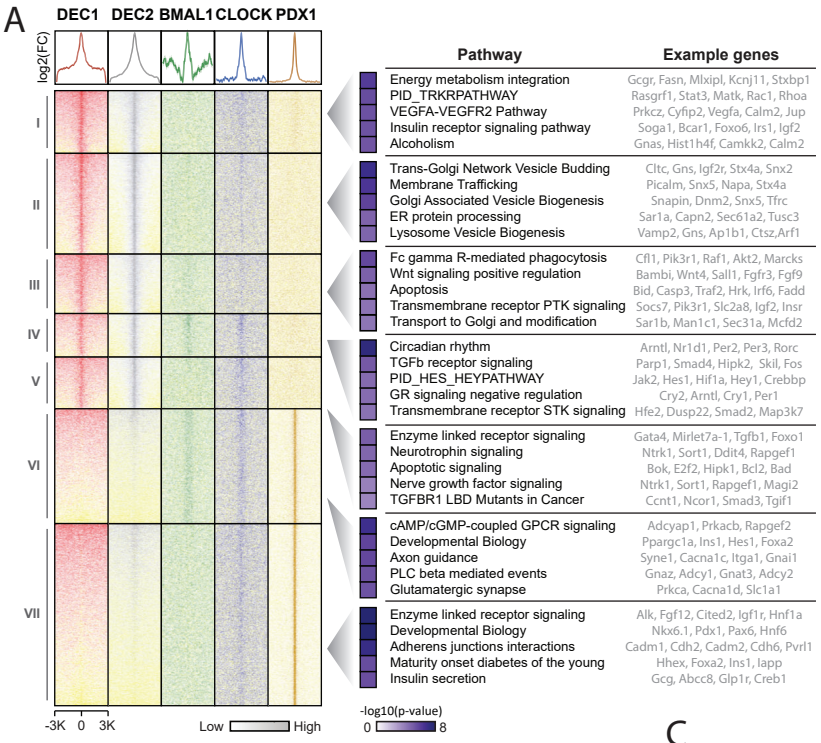
A
DEC1 DEC2 BMAL1 CLOCK PDX1
log2(FC)
I
II
III
IV
V
VI
VII
-3K 0 3K
Low High
-log10(p-value)
0 8
Pathway
Example genes
Energy metabolism integration
PID_TRKRPATHWAY
VEGFA-VEGFR2 Pathway
Insulin receptor signaling pathway
Alcoholism
Gcgr, Fasn, Mlxipl, Kcnj11, Stxbp1
Rasgrf1, Stat3, Matk, Rac1, Rhoa
Prkcz, Cyfip2, Vegfa, Calm2, Jup
Soga1, Bcar1, Foxo6, Irs1, Igf2
Gnas, Hist1h4f, Camkk2, Calm2
Trans-Golgi Network Vesicle Budding
Membrane Trafficking
Golgi Associated Vesicle Biogenesis
ER protein processing
Lysosome Vesicle Biogenesis
Cltc, Gns, Igf2r, Stx4a, Snx2
Picalm, Snx5, Napa, Stx4a
Snapin, Dnm2, Snx5, Tfrc
Sar1a, Capn2, Sec61a2, Tusc3
Vamp2, Gns, Ap1b1, Ctsz,Arf1
Fc gamma R-mediated phagocytosis
Wnt signaling positive regulation
Apoptosis
Transmembrane receptor PTK signaling
Transport to Golgi and modification
Cfl1, Pik3r1, Raf1, Akt2, Marcks
Bambi, Wnt4, Sall1, Fgfr3, Fgf9
Bid, Casp3, Traf2, Hrk, Irf6, Fadd
Socs7, Pik3r1, Slc2a8, Igf2, Insr
Sar1b, Man1c1, Sec31a, Mcfd2
Circadian rhythm
TGFb receptor signaling
PID_HES_HEYPATHWAY
GR signaling negative regulation
Transmembrane receptor STK signaling
Arntl, Nr1d1, Per2, Per3, Rorc
Parp1, Smad4, Hipk2, Skil, Fos
Jak2, Hes1, Hif1a, Hey1, Crebbp
Cry2, Arntl, Cry1, Per1
Hfe2, Dusp22, Smad2, Map3k7
Enzyme linked receptor signaling
Neurotrophin signaling
Apoptotic signaling
Nerve growth factor signaling
TGFBR1 LBD Mutants in Cancer
Gata4, Mirlet7a-1, Tgfb1, Foxo1
Ntrk1, Sort1, Ddit4, Rapgef1
Bok, E2f2, Hipk1, Bcl2, Bad
Ntrk1, Sort1, Rapgef1, Magi2
Ccnt1, Ncor1, Smad3, Tgif1
cAMP/cGMP-coupled GPCR signaling
Developmental Biology
Axon guidance
PLC beta mediated events
Glutamatergic synapse
Adcyap1, Prkacb, Rapgef2
Ppargc1a, Ins1, Hes1, Foxa2
Syne1, Cacna1c, Itga1, Gnai1
Gnaz, Adcy1, Gnat3, Adcy2
Prkca, Cacna1d, Slc1a1
Enzyme linked receptor signaling
Developmental Biology
Adherens junctions interactions
Maturity onset diabetes of the young
Insulin secretion
Alk, Fgf12, Cited2, Igf1r, Hnf1a
Nkx6.1, Pdx1, Pax6, Hnf6
Cadm1, Cdh2, Cadm2, Cdh6, Pvrl1
Hhex, Foxa2, Ins1, Iapp
Gcg, Abcc8, Glp1r, Creb1

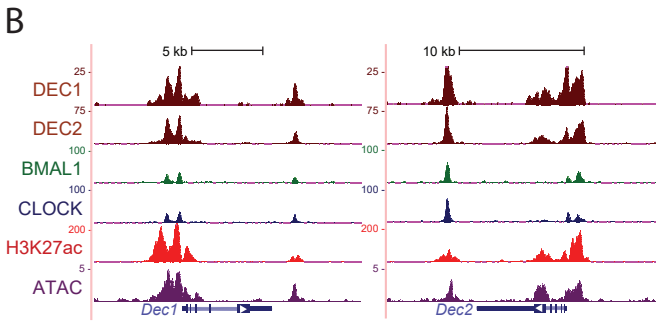
B
5 kb
10 kb
DEC1
DEC2
BMAL1
CLOCK
H3K27ac
ATAC
Dec1
Dec2

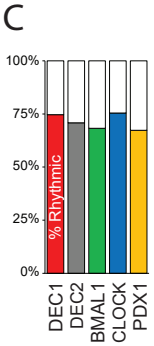
C
100%
75%
50%
25%
0%
% Rhythmic
DEC1
DEC2
BMAL1
CLOCK
PDX1

**Figure 3. DEC1 selectively binds rhythmic energy metabolism and secretory genes in β-cells.**

(**A**) Left: density of ChIP-seq signal enrichment over input ±3kb around the center of each DEC1, DEC2, BMAL1, CLOCK, and PDX1 binding peak in β-cells. Right: pathways enriched among genes linked to binding peaks for DEC1, DEC2, BMAL1, CLOCK, and PDX1 in β-cells.

(**B**) Genomic view of DEC1, DEC2, BMAL1, and CLOCK binding at *Dec1* and *Dec2* loci in β-cells. Tracks display normalized ChIP and ATAC sequencing read density. Gene models are shown below.

(**C**) Fraction of DEC1, DEC2, BMAL1, CLOCK, and PDX1 target genes expressed rhythmically in β-cells. Rhythmicity analysis, dryR.

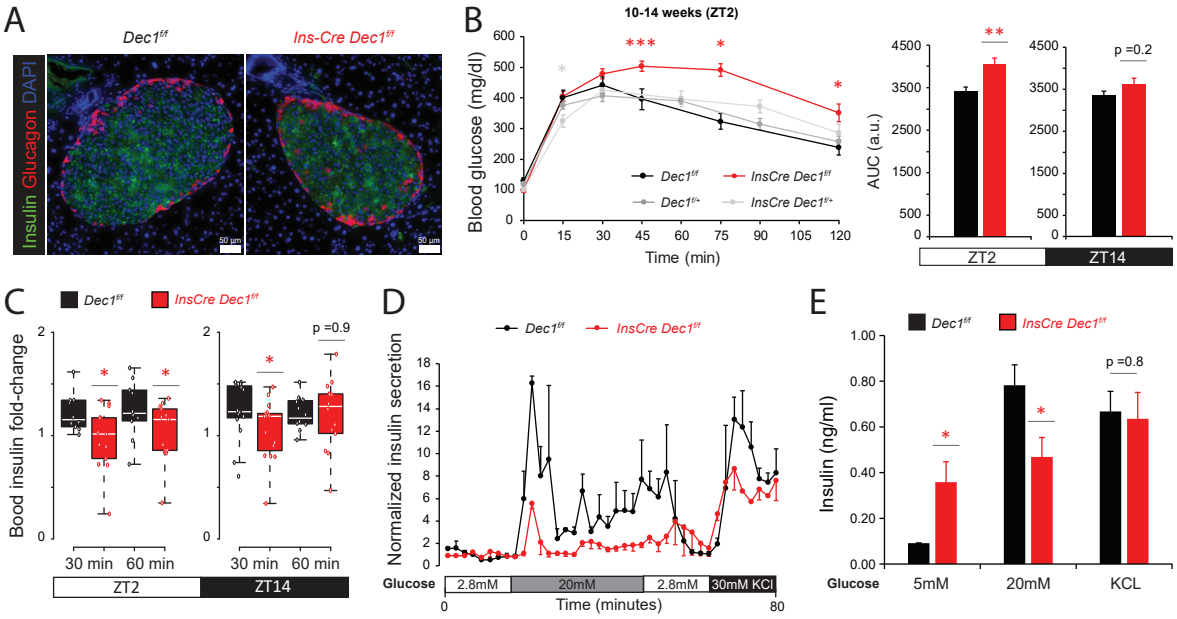
A
Dec1f/f
Ins-Cre Dec1f/f
Insulin Glucagon DAPI
50 µm
B
10-14 weeks (ZT2)
Blood glucose (mg/dl)
Time (min)
Dec1f/f
InsCre Dec1f/f
Dec1f/+
InsCre Dec1f/+
AUC (a.u.)
p =0.2
ZT2
ZT14
C
Dec1f/f
InsCre Dec1f/f
Bood insulin fold-change
p =0.9
30 min
60 min
ZT2
ZT14
D
Dec1f/f
InsCre Dec1f/f
Normalized insulin secretion
Glucose
2.8mM
20mM
2.8mM
30mM KCl
Time (minutes)
E
Dec1f/f
InsCre Dec1f/f
Insulin (ng/ml)
p =0.8
Glucose
5mM
20mM
KCL

**Figure 4. β-cell DEC1 loss causes insulin deficiency and glucose intolerance due to islet immaturity.**

(**A**) Immunofluorescence staining of insulin (green), glucagon (red), and DAPI (blue) in *Dec1*$^{f/f}$ and *InsCre Dec1*$^{f/f}$ mice pancreata.

(**B**) Glucose tolerance in 14-hour fasted N =20 *InsCre Dec1*$^{f/f}$, 17 *Dec1*$^{f/f}$, 12 *InsCre Dec1*$^{f/+}$, and 9 *Dec1*$^{f/+}$ mice 3-month-old mice following intraperitoneal glucose administration at ZT2 (left, middle) and ZT14 (right). Data are mean ±SEM.

(**C**) Blood insulin secretion fold-change in 14-hour fasted N =13-15 *InsCre Dec1*$^{f/f}$ and 10-15 *Dec1*$^{f/f}$ 2-3-month-old mice following intraperitoneal glucose administration at ZT2 (left) and ZT14 (right).

(**D**) Glucose-stimulated insulin secretion dynamics in perifused islets from N =2 *InsCre Dec1*$^{f/f}$ and 2 *Dec1*$^{f/f}$ mice, each with n =2-4 replicate measurements of 20 similar-sized islets. Data are mean ±SEM, normalized to the mean of the first incubation.

(**E**) Insulin secretion of isolated islets from N =10 *InsCre Dec1*$^{f/f}$ and 9 *Dec1*$^{f/f}$ mice, each with n =2 replicate measurements of 20 size-matched islets under the indicated parallel static incubations. Data are mean ±SEM.

*p <0.05, **p <1e-2, ***p <1e-3, t test.

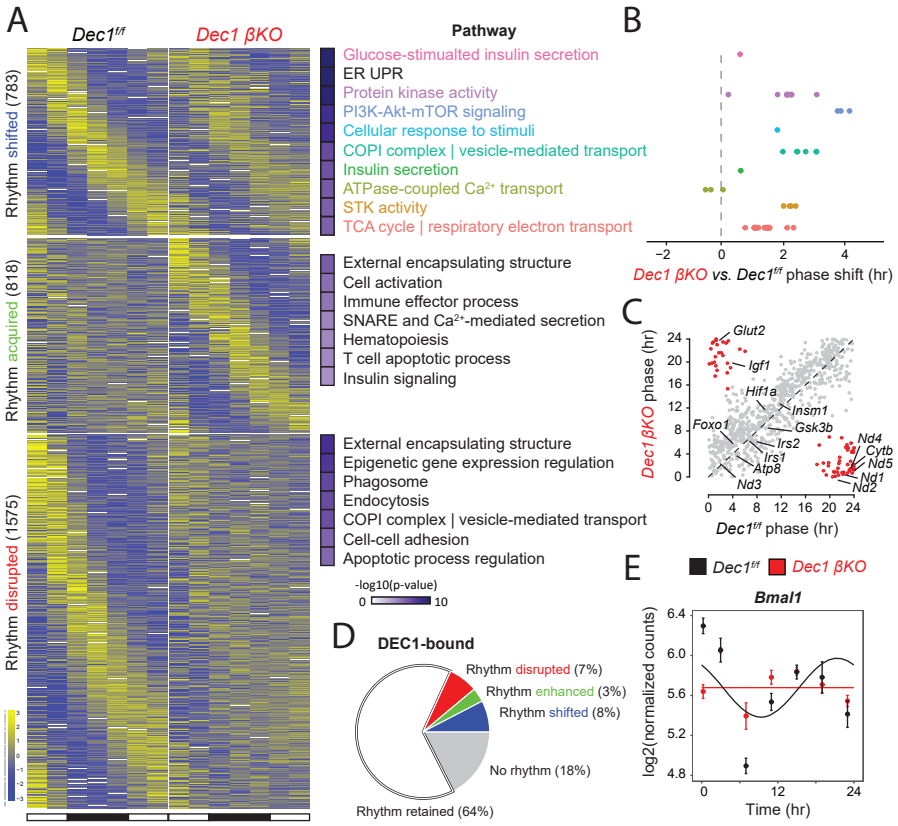
A
Dec1f/f
Dec1 βKO
Pathway
Rhythm shifted (783)
Glucose-stimualted insulin secretion
ER UPR
Protein kinase activity
PI3K-Akt-mTOR signaling
Cellular response to stimuli
COPI complex | vesicle-mediated transport
Insulin secretion
ATPase-coupled Ca2+ transport
STK activity
TCA cycle | respiratory electron transport
Rhythm acquired (818)
External encapsulating structure
Cell activation
Immune effector process
SNARE and Ca2+-mediated secretion
Hematopoiesis
T cell apoptotic process
Insulin signaling
Rhythm disrupted (1575)
External encapsulating structure
Epigenetic gene expression regulation
Phagosome
Endocytosis
COPI complex | vesicle-mediated transport
Cell-cell adhesion
Apoptotic process regulation
-log10(p-value)
0
10
B
−2
0
2
4
Dec1 βKO vs. Dec1f/f phase shift (hr)
C
Glut2
Igf1
Hif1a
Insm1
Foxo1
Gsk3b
Irs2
Irs1
Atp8
Nd3
Nd4
Cytb
Nd5
Nd1
Nd2
Dec1 βKO phase (hr)
Dec1f/f phase (hr)
D
DEC1-bound
Rhythm disrupted (7%)
Rhythm enhanced (3%)
Rhythm shifted (8%)
No rhythm (18%)
Rhythm retained (64%)
E
Dec1f/f
Dec1 βKO
Bmal1
log2(normalized counts)
6.4
6.0
5.6
5.2
4.8
0
12
24
Time (hr)

**Figure 5. DEC1 synchronizes respiratory metabolism and insulin secretion gene rhythms in pancreatic β-cells.**

(**A-B**) Expression of genes whose rhythm is disrupted (bottom), enhanced (middle), or shifted (top) in islets isolated and pooled from N =2 *Dec1-βKO* and 2 *Dec1*$^{f/f}$ mice (A, left), highlighting enriched pathways (A, right), and average phase change for pathways enriched among rhythm-shifted genes, colored by biological theme (B). Data are mean from n =4 replicate measurements.

(**C**) Phase change for individual rhythm-shifted genes, highlighting mediators of glucose sensing, metabolism, and insulin secretion.

(**D**) Fraction of DEC1-bound genes with non-rhythmic (gray) or rhythmic expression that is retained (white), disrupted (red), enhanced (green) or shifted (blue) in *Dec1-βKO* mice.

(**E**) Temporal expression pattern of *Bmal1* in islets isolated and pooled from N =2 *Dec1-βKO* and 2 *Dec1*$^{f/f}$ mice. Data are mean ±SEM from n =4 replicate measurements.

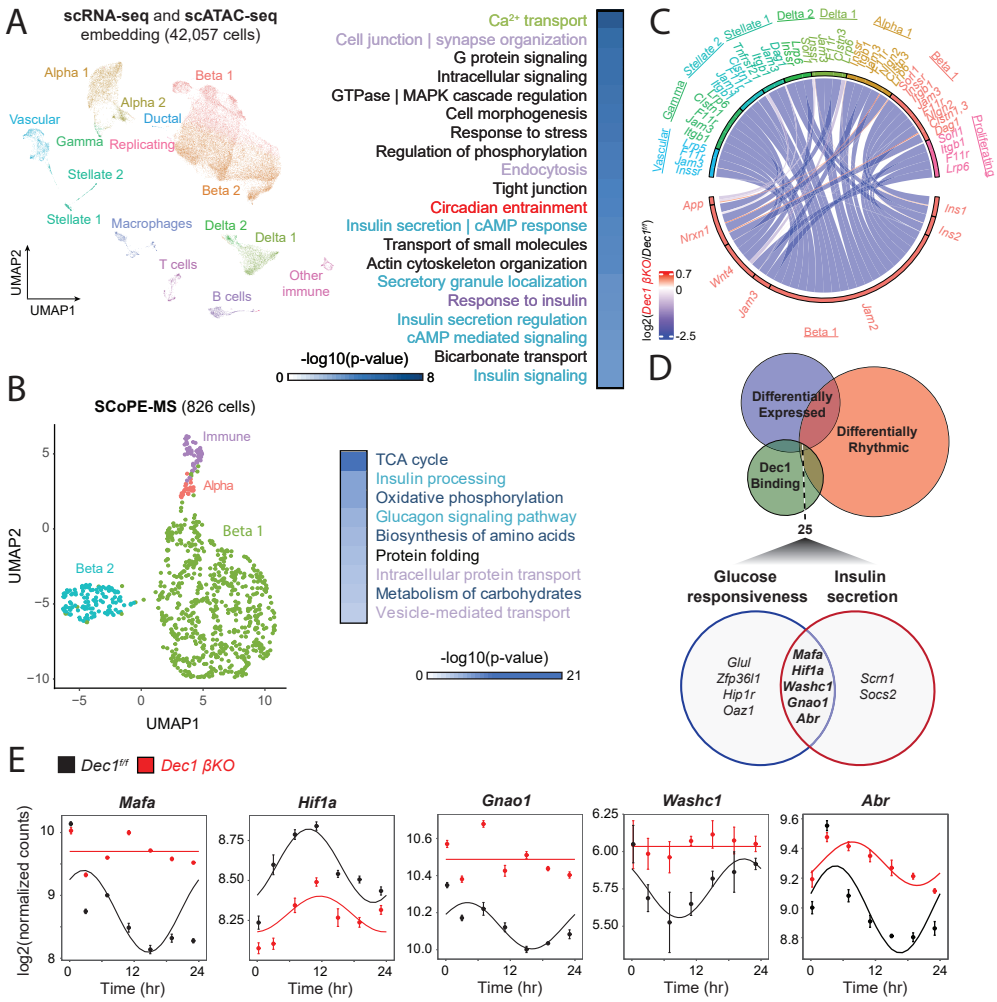
A
scRNA-seq and scATAC-seq
embedding (42,057 cells)
Alpha 1
Beta 1
Alpha 2
Ductal
Vascular
Gamma
Replicating
Stellate 2
Beta 2
Stellate 1
Macrophages
Delta 2
Delta 1
T cells
Other immune
B cells
UMAP2
UMAP1
Ca2+ transport
Cell junction | synapse organization
G protein signaling
Intracellular signaling
GTPase | MAPK cascade regulation
Cell morphogenesis
Response to stress
Regulation of phosphorylation
Endocytosis
Tight junction
Circadian entrainment
Insulin secretion | cAMP response
Transport of small molecules
Actin cytoskeleton organization
Secretory granule localization
Response to insulin
Insulin secretion regulation
cAMP mediated signaling
Bicarbonate transport
Insulin signaling
-log10(p-value)
0
8
C
Stellate 1
Delta 2
Delta 1
Alpha 1
Beta 1
Stellate 2
Gamma
Vascular
Proliferating
App
Nrxn1
Wnt4
Jam3
Jam2
Ins1
Ins2
Beta 1
log2(Dec1 βKO/Dec1f/f)
0.7
0
-2.5
B
SCoPE-MS (826 cells)
Immune
Alpha
Beta 1
Beta 2
UMAP2
UMAP1
TCA cycle
Insulin processing
Oxidative phosphorylation
Glucagon signaling pathway
Biosynthesis of amino acids
Protein folding
Intracellular protein transport
Metabolism of carbohydrates
Vesicle-mediated transport
-log10(p-value)
0
21
D
Differentially Expressed
Differentially Rhythmic
Dec1 Binding
25
Glucose responsiveness
Insulin secretion
Glul
Zfp36l1
Hip1r
Oaz1
Mafa
Hif1a
Washc1
Gnao1
Abr
Scrn1
Socs2
E
Dec1f/f
Dec1 βKO
Mafa
Hif1a
Gnao1
Washc1
Abr
log2(normalized counts)
Time (hr)

**Figure 6. DEC1 regulates coupling of insulin secretion to glucose, shaping islet cell-cell coordination.**

(**A**) Co-embedding of single-cell open chromatin (scATAC-seq) and gene expression (scRNA-seq) profiles in islets isolated from N =2 *Dec1-βKO* and 2 *Dec1*$^{f/f}$ mice, each sequenced separately (left). Pathways enriched among genes deregulated at both chromatin and transcription levels (right).

(**B**) Single-cell clustering by protein expression profiles, assayed by SCoPE-MS, in islets isolated from N =2 *Dec1-βKO* and 2 littermate control mice, each run separately (left). Pathways enriched among differentially regulated proteins (right).

(**C**) Ligand-receptor interaction analysis showing 7 of the top 10 differentially active interactions, where ligand expression is significantly altered in Beta 1 cells with higher expression of insulin and maturity markers.

(**D**) Overlap between DEC1-bound genes in β cells and genes that are differentially rhythmic and differentially expressed in β cells from *Dec1-βKO* mice, highlighting the significant enrichment in shared genes mediating glucose responsiveness and insulin secretion.

(**E**) Temporal expression pattern of *Mafa, Hif1a, Gnao1, Washc1, and Abr* in islets isolated and pooled from N =2 *Dec1-βKO* and 2 *Dec1*$^{f/f}$ mice. Data are mean ±SEM from n =4 replicate measurements.

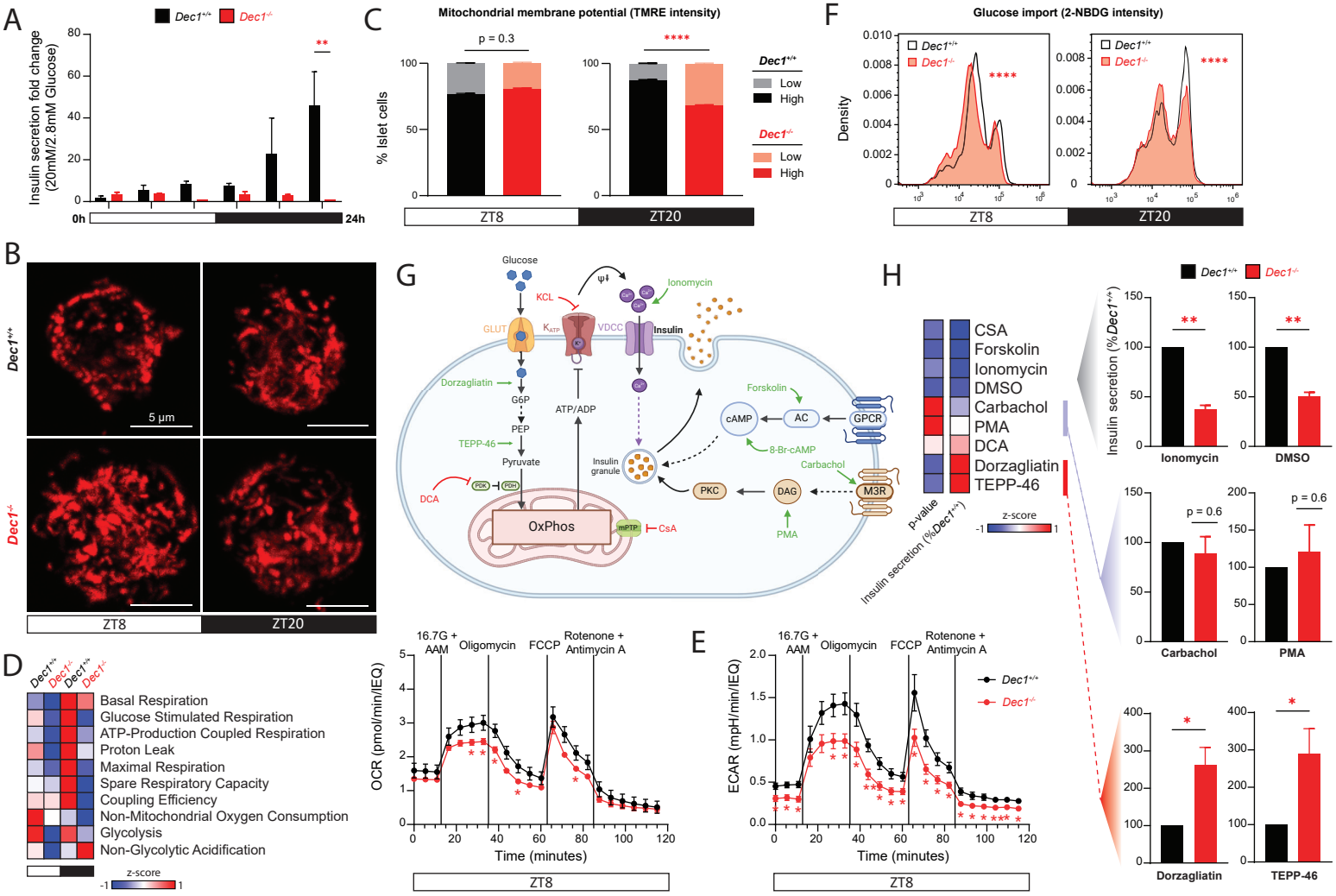
A
Dec1+/+
Dec1-/-
Insulin secretion fold change (20mM/2.8mM Glucose)
0h
24h
B
Dec1+/+
Dec1-/-
5 µm
ZT8
ZT20
C
Mitochondrial membrane potential (TMRE intensity)
p = 0.3
****
% Islet cells
Low
High
ZT8
ZT20
D
Basal Respiration
Glucose Stimulated Respiration
ATP-Production Coupled Respiration
Proton Leak
Maximal Respiration
Spare Respiratory Capacity
Coupling Efficiency
Non-Mitochondrial Oxygen Consumption
Glycolysis
Non-Glycolytic Acidification
z-score
E
16.7G + AAM
Oligomycin
FCCP
Rotenone + Antimycin A
OCR (pmol/min/IEQ)
ECAR (mpH/min/IEQ)
Time (minutes)
ZT8
F
Glucose import (2-NBDG intensity)
Density
ZT8
ZT20
G
Glucose
KCL
Ionomycin
GLUT
Insulin
VDCC
Dorzagliatin
G6P
PEP
Pyruvate
TEPP-46
ATP/ADP
Forskolin
cAMP
AC
GPCR
8-Br-cAMP
Carbachol
Insulin granule
PKC
DAG
M3R
PMA
DCA
OxPhos
CsA
H
CSA
Forskolin
Ionomycin
DMSO
Carbachol
PMA
DCA
Dorzagliatin
TEPP-46
p-value
Insulin secretion (%Dec1+/+)
z-score
Ionomycin
DMSO
p = 0.6
Carbachol
PMA
Dorzagliatin
TEPP-46

**Figure 7. A deficit in circadian bioenergetics underlies immature β-cell function upon DEC1 loss.**

(**A**) Insulin secretion fold-change between 2.8mM and 20mM glucose sequential static incubations of islets isolated from *Dec1*$^{+/+}$ and *Dec1*$^{-/-}$ mice assayed at 4h intervals for 20h. Data are mean ±SEM from n =2-3 replicate measurements of 20 size-matched islets.

(**B**) Confocal imagining of mitochondria stained with MitoTracker Red CMXRos at ZT8 and ZT20 in β-cells isolated from *Dec1*$^{+/+}$ and *Dec1*$^{-/-}$ mice.

(**C**) Proportion of β-cells isolated from *Dec1*$^{+/+}$ and *Dec1*$^{-/-}$ mice with low and high mitochondrial membrane potential determined by TMRE staining at ZT8 and ZT20. Data are mean ±SEM from n=4 replicate measurements, each with >10,000 cells.

(**D-E**) Metabolic flux at ZT8 and ZT20 in islets isolated from *Dec1*$^{+/+}$ and *Dec1*$^{-/-}$ mice (D, left) quantified from measurements of oxygen consumption rate (OCR) (D, right) and extracellular acidification rate (ECAR) (E) in response to 16.7mM glucose and a physiological amino acid mixture (16.7G + AAM), oligomycin, FCCP, and to rotenone and antimycin A at the indicated times. Data are mean ±SEM from n =4-7 replicate measurements of 12 similar-sized islets.

(**F**) Glucose uptake in β-cells isolated from *Dec1*$^{+/+}$ and *Dec1*$^{-/-}$ mice quantified by import of the fluorescent glucose analog 2-NBDG at ZT8 and ZT20. Data are distributions from n=2 replicate measurements, each with >10,000 cells.

(**G-H**) Screen of insulinotropic agents to rescue the GSIS defect of isolated *Dec1*$^{-/-}$ and *Dec1*-βKO islets (G), and results for significance and fold-change in insulin secretion between 2.8mM and 20mM glucose sequential static incubations of *Dec1*$^{-/-}$ relative to *Dec1*$^{+/+}$ islets (H, left), with the relative vehicle (DMSO) or secretagogue-stimulated insulin secretion shown to the right (H, right). Data are mean ±SEM from N =2-4 mice, each with n =2-3 replicate measurements of size-matched islets, normalized to intracellular insulin content.

*p <0.05, **p <1e-2, ****p <1e-4, ANOVA test (A), Pearson's Chi-squared test (C), t test [(D), (E), (H)], and Wilcoxon test (F).

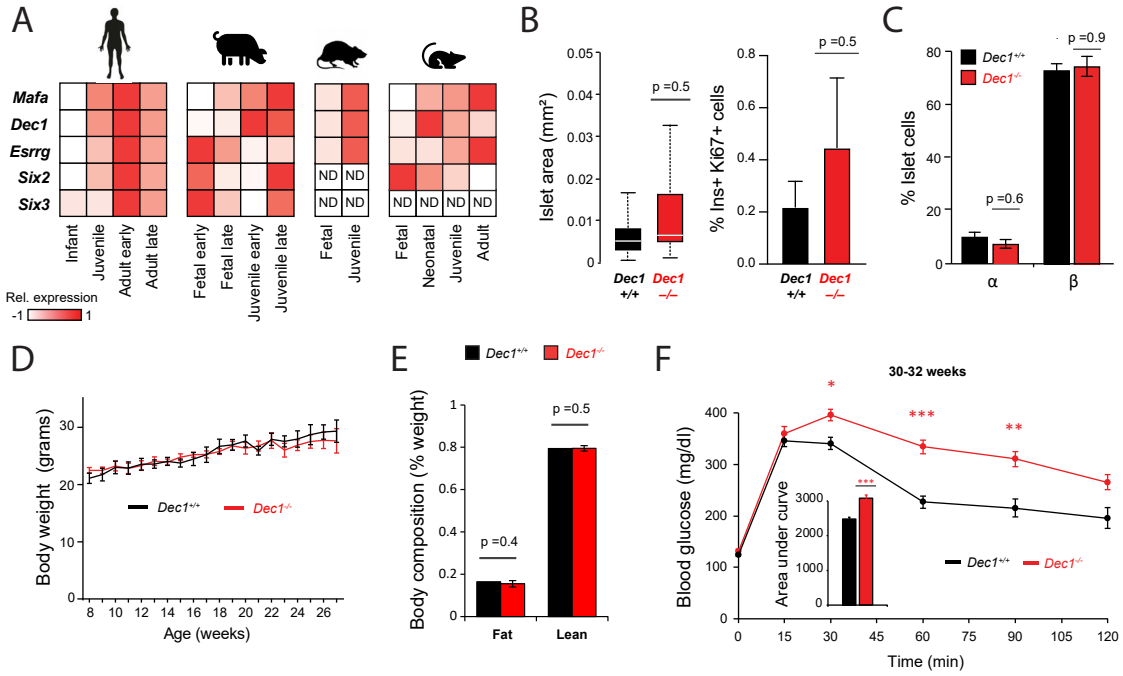
A
Mafa
Dec1
Esrrg
Six2
Six3
ND
Infant
Juvenile
Adult early
Adult late
Fetal early
Fetal late
Juvenile early
Juvenile late
Fetal
Juvenile
Fetal
Neonatal
Juvenile
Adult
Rel. expression
-1
1
B
Islet area (mm²)
p =0.5
Dec1 +/+
Dec1 −/−
% Ins+ Ki67+ cells
p =0.5
C
% Islet cells
Dec1+/+
Dec1-/-
p =0.9
p =0.6
α
β
D
Body weight (grams)
Dec1+/+
Dec1-/-
Age (weeks)
E
Dec1+/+
Dec1-/-
Body composition (% weight)
p =0.4
p =0.5
Fat
Lean
F
30-32 weeks
Blood glucose (mg/dl)
Area under curve
Dec1+/+
Dec1-/-
Time (min)

**Figure S1. DEC1 defines mature β cells and impacts blood glucose tolerance despite normal islet formation and body metrics.**

(**A**) Developmental stage specificity of *Dec1* for adult β cells in N =2-3 humans, 2-11 pigs, 3 rats, and 1-3 mice, compared to adult-restricted transcription factors known to regulate human β-cell functional maturation. Data are mean from unsynchronized β cells.

(**B**) Islet area (left) and mean ±SEM fraction of proliferating (Ki67+) beta cells (right) in n =24 *Dec1*$^{+/+}$ and 11 *Dec1*$^{-/-}$ islets pooled from N =1-2 mice pancreata.

(**C**) Proportion of alpha and beta cells in n =24 *Dec1*$^{+/+}$ and 11 *Dec1*$^{-/-}$ islets pooled from N =1-2 mice pancreata.

(**D**) Weight of *ad libitum* fed N =16 *Dec1*$^{+/+}$ and 12 *Dec1*$^{-/-}$ mice at ZT12 monitored from age 8-27 weeks. Data are mean ±SEM.

(**E**) Body composition of *Dec1*$^{+/+}$ and *Dec1*$^{-/-}$ 9-10-month-old mice. Data are mean ±SEM of N =1-5 mice.

(**F**) Glucose tolerance in 14-hour fasted N =12 *Dec1*$^{+/+}$ and 25 *Dec1*$^{-/-}$ 8-month-old mice following intraperitoneal glucose administration at ZT2. Data are mean ±SEM.

*p <0.05, **p <0.01, ***p <0.001, t test.

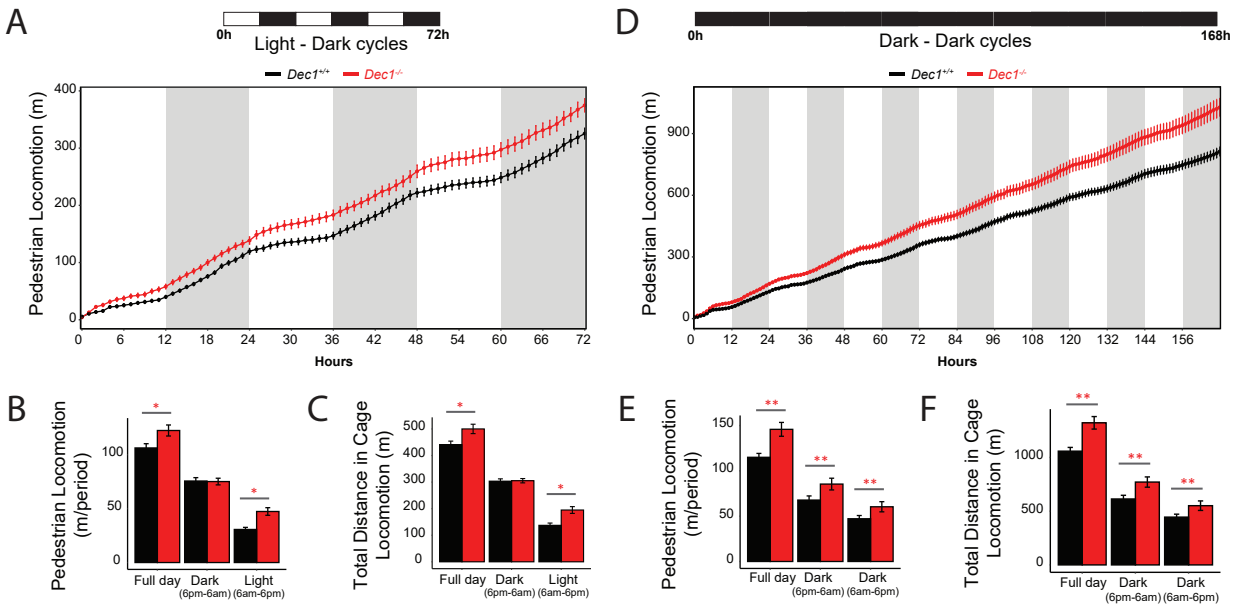
A
0h
Light - Dark cycles
72h
Dec1+/+
Dec1-/-
Pedestrian Locomotion (m)
Hours
D
0h
Dark - Dark cycles
168h
Dec1+/+
Dec1-/-
Pedestrian Locomotion (m)
Hours
B
Pedestrian Locomotion (m/period)
Full day
Dark (6pm-6am)
Light (6am-6pm)
C
Total Distance in Cage Locomotion (m)
Full day
Dark (6pm-6am)
Light (6am-6pm)
E
Pedestrian Locomotion (m/period)
Full day
Dark (6pm-6am)
Dark (6am-6pm)
F
Total Distance in Cage Locomotion (m)
Full day
Dark (6pm-6am)
Dark (6am-6pm)

**Figure S2. *Dec1* disruption impacts pedestrian locomotor activity**

(**A**) Cumulative pedestrian locomotion of N =13 *Dec1*$^{+/+}$ and 14 *Dec1*$^{-/-}$ mice across 3 days in 12-hour light-dark cycles.

(**B-C**) Overall daily values by genotype and photoperiod for pedestrian locomotion (B) and total distance in cage (C) measurements. Data are mean ±SEM.

(**D**) Cumulative pedestrian locomotion of N =13 *Dec1*$^{+/+}$ and 14 *Dec1*$^{-/-}$ mice across 7 days in 12-hour dark-dark cycles.

(**E-F**) Overall daily values by genotype and subjective photoperiod for pedestrian locomotion (E) and total distance in cage (F) measurements. Data are mean ±SEM.

*p <0.05, **p <0.01, ANOVA test.

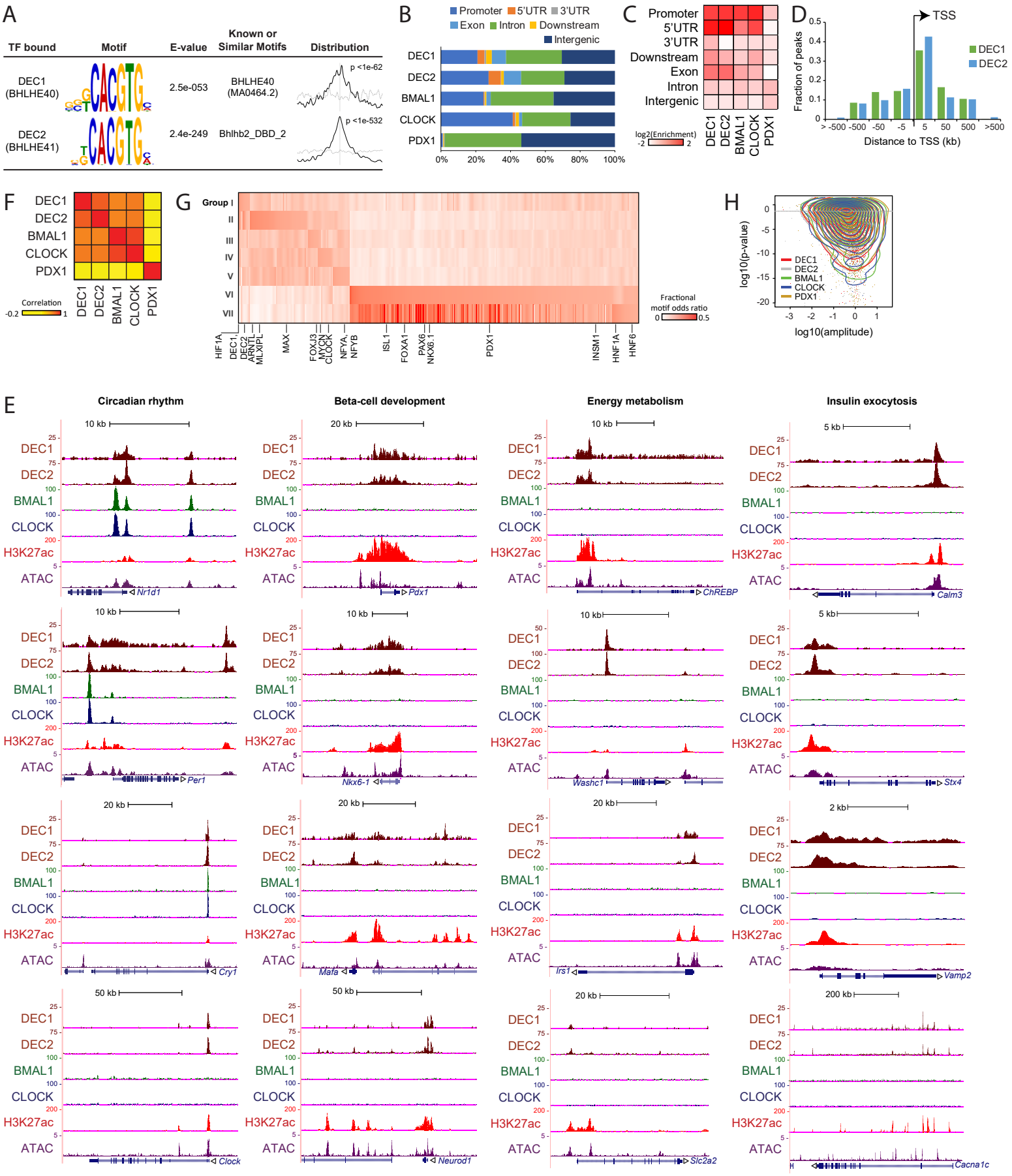
A
TF bound
Motif
E-value
Known or Similar Motifs
Distribution
DEC1 (BHLHE40)
2.5e-053
BHLHE40 (MA0464.2)
p <1e-62
DEC2 (BHLHE41)
2.4e-249
Bhlhb2_DBD_2
p <1e-532
B
Promoter
5'UTR
3'UTR
Exon
Intron
Downstream
Intergenic
DEC1
DEC2
BMAL1
CLOCK
PDX1
0%
20%
40%
60%
80%
100%
C
Promoter
5'UTR
3'UTR
Downstream
Exon
Intron
Intergenic
log2(Enrichment)
-2
2
D
TSS
Fraction of peaks
Distance to TSS (kb)
> -500
-500
-50
-5
5
50
500
>500
F
Correlation
-0.2
1
G
Group I
II
III
IV
V
VI
VII
Fractional motif odds ratio
0
0.5
HIF1A
DEC1
DEC2
ARNTL
MLXIPL
MAX
FOXJ3
MYCN
CLOCK
NFYA
NFYB
ISL1
FOXA1
PAX6
NKX6.1
PDX1
INSM1
HNF1A
HNF6
H
log10(p-value)
log10(amplitude)
E
Circadian rhythm
Beta-cell development
Energy metabolism
Insulin exocytosis
DEC1
DEC2
BMAL1
CLOCK
H3K27ac
ATAC
Nr1d1
Pdx1
ChREBP
Calm3
Per1
Nkx6-1
Washc1
Stx4
Cry1
Mafa
Irs1
Vamp2
Clock
Neurod1
Slc2a2
Cacna1c

**Figure S3. Circadian clock DEC components selectively bind to energy metabolism and insulin secretion genes.**

(**A**) DEC1 and DEC2 binding peaks identified by ChIP-seq in β-cells enrich for the known DEC1 and DEC2 recognition motifs, respectively. Shown are the top motif identified by MEME-ChIP (*52*) across peak regions, its significance (E-value), top known motif match, and the distribution of the best matches to the motif across center-aligned peak regions.

(**B**) Distribution of genomic locations for DEC1, DEC2, BMAL1, CLOCK, and PDX1 binding peaks from ChIP-seq in β-cells.

(**C**) Relative enrichment for genomic locations among DEC1, DEC2, BMAL1, CLOCK, and PDX1 binding peaks from ChIP-seq in β-cells.

(**D**) Distance to the nearest TSS for DEC1, DEC2, BMAL1, CLOCK, and PDX1 binding peaks from ChIP-seq in β-cells.

(**E**) Genomic view of DEC1, DEC2, BMAL1, and CLOCK binding in β-cells at genes regulating circadian rhythm, beta-cell development, energy metabolism, and insulin exocytosis. Tracks display normalized ChIP and ATAC sequencing read density. Gene models are shown below.

(**F**) Correlation between DEC1, DEC2, BMAL1, CLOCK, and PDX1 ChIP-seq signal, calculated across the union of their respective binding peaks.

(**G**) Transcription factor motifs enriched in ChIP-seq clusters I to VII from Figure 3A. Heatmap shows relative enrichment across the groups for all motifs with group-specific expression.

(**H**) Relationship between expression amplitude (peak-to-trough ratio), and significance of rhythmicity, as assessed by dryR (*13*), for all genes linked to DEC1, DEC2, BMAL1, CLOCK, and PDX1 binding peaks from ChIP-seq in β-cells, indicating the $p < 0.05$ threshold used.

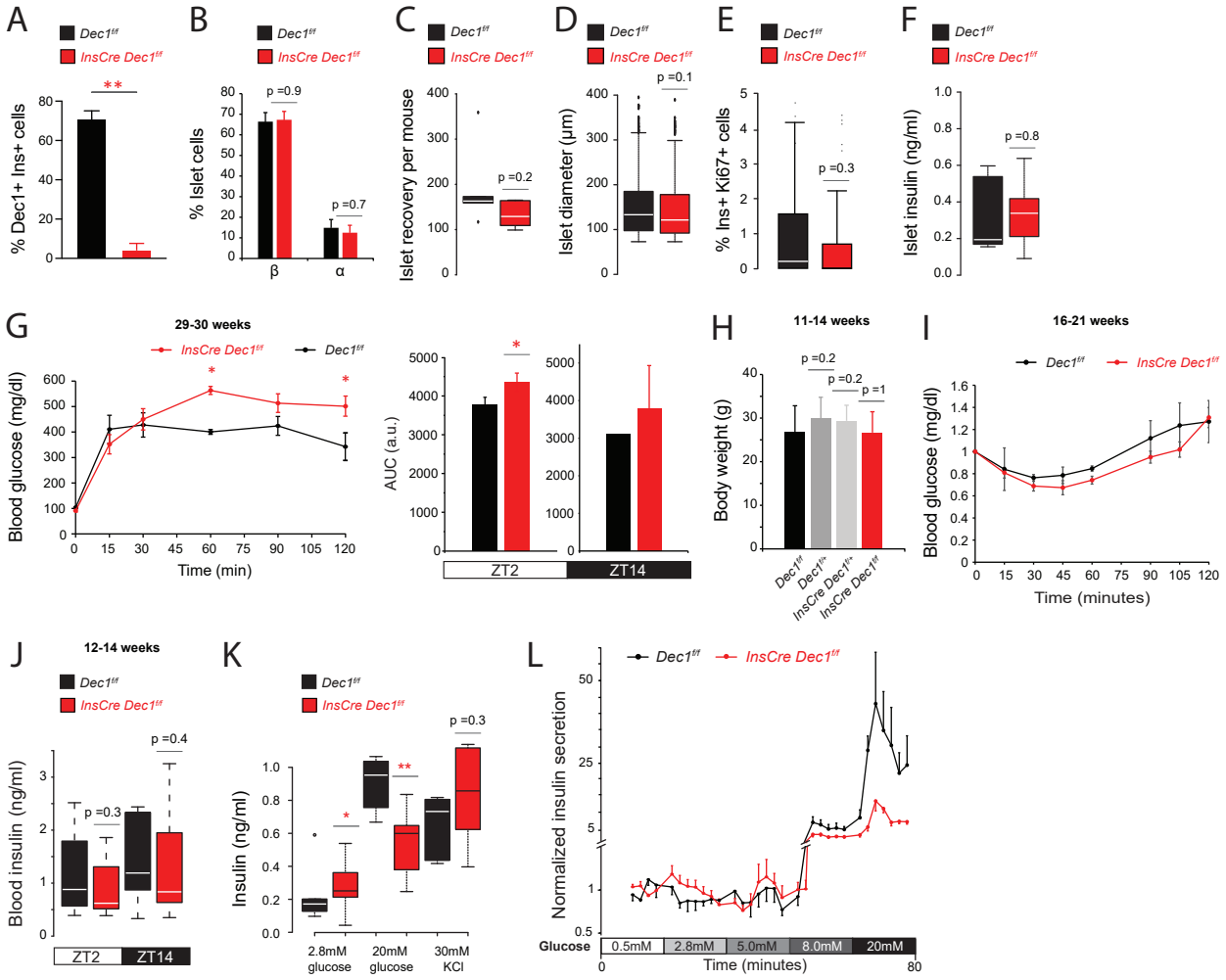
A
Dec1f/f
InsCre Dec1f/f
% Dec1+ Ins+ cells
**
B
% Islet cells
p =0.9
p =0.7
β
α
C
Islet recovery per mouse
p =0.2
D
Islet diameter (µm)
p =0.1
E
% Ins+ Ki67+ cells
p =0.3
F
Islet insulin (ng/ml)
p =0.8
G
29-30 weeks
Blood glucose (mg/dl)
Time (min)
AUC (a.u.)
ZT2
ZT14
H
11-14 weeks
Body weight (g)
p =0.2
p =0.2
p =1
Dec1f/f
Dec1f/+
InsCre Dec1f/+
InsCre Dec1f/f
I
16-21 weeks
Blood glucose (mg/dl)
Time (minutes)
J
12-14 weeks
Blood insulin (ng/ml)
p =0.3
p =0.4
ZT2
ZT14
K
Insulin (ng/ml)
p =0.3
2.8mM glucose
20mM glucose
30mM KCl
L
Normalized insulin secretion
Glucose
0.5mM
2.8mM
5.0mM
8.0mM
20mM
Time (minutes)

**Figure S4. Glucose intolerance and immature islet function in young and aged β-cell specific *Dec1*-mutant mice despite normal weight, insulin sensitivity, and islet formation.**

(**A**) Fraction of DEC1-positive beta cells in islets from N =1 *InsCre Dec1*$^{f/f}$ and 1 *Dec1*$^{f/f}$ mice pancreata. Data are mean ±SEM from n =2 replicate measurements.

(**B**) Proportion of alpha and beta cells in isolated islets pooled from N =2 *InsCre Dec1*$^{f/f}$ and 3 *Dec1*$^{f/f}$ mice. Data are mean ±SEM.

(**C**) Islets isolated from each of N =5 *InsCre Dec1*$^{f/f}$ and 5 *Dec1*$^{f/f}$ mice.

(**D**) Diameter of islets isolated from each of N =5 *InsCre Dec1*$^{f/f}$ and 5 *Dec1*$^{f/f}$ mice.

(**E**) Fraction of proliferating (Ki67+) beta cells in n =39 *InsCre Dec1*$^{f/f}$ and 31 *Dec1*$^{f/f}$ mice islets pooled from N =1-2 mice pancreata.

(**F**) Insulin content of isolated *InsCre Dec1*$^{f/f}$ islets. Data are pooled from N =6 *InsCre Dec1*$^{f/f}$ and 6 *Dec1*$^{f/f}$ mice.

(**G**) Glucose tolerance in 14-hour fasted N =20 *InsCre Dec1*$^{f/f}$ and 17 *Dec1*$^{f/f}$ 8-month-old mice following intraperitoneal glucose administration at ZT2. Data are mean ±SEM.

(**H**) Weight of 14-hour fasted N =20 *InsCre Dec1*$^{f/f}$, 17 *Dec1*$^{f/f}$, 12 *InsCre Dec1*$^{f/+}$, and 9 *Dec1*$^{f/+}$ 2-3-month-old mice at ZT2. Data are mean ±SEM.

(**I**) Insulin tolerance N =3 *InsCre Dec1*$^{f/f}$ and 3 *Dec1*$^{f/f}$ 4-5-month-old mice following intraperitoneal insulin administration at ZT2. Data are mean ±SEM.

(**J**) Blood insulin in *ad libitum* fed N =12 *InsCre Dec1*$^{f/f}$ and 8 *InsCre Dec1*$^{f/f}$ 3-month-old mice at ZT2 and ZT14. Data are mean of n =2 replicate measurements.

(**K**) Glucose-stimulated insulin secretion of isolated islets from N =6 *InsCre Dec1*$^{f/f}$ and 6 *Dec1*$^{f/f}$ mice, each with n =2 replicate measurements of 20 size-matched islets under the indicated sequential static incubations.

(**L**) Insulin secretion dynamics in perifused islets from N =2 *InsCre Dec1*$^{f/f}$ and 2 *Dec1*$^{f/f}$ mice, each with n =3 replicate measurements of 20 size-matched islets under increasing glucose concentrations. Data are mean ±SEM, normalized to the mean of the first incubation.

*p <0.05, **p <0.01, t test.

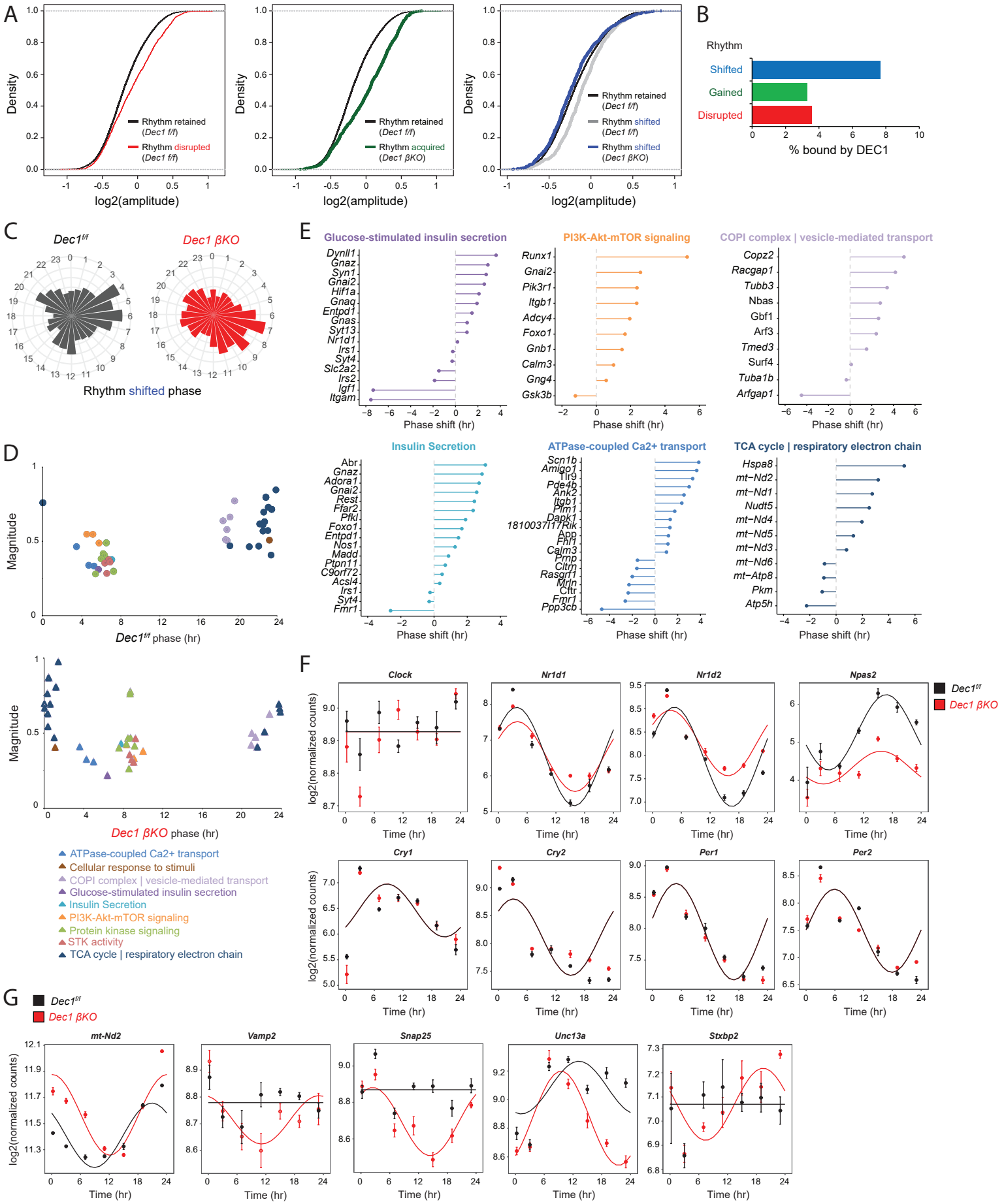
A
Density
log2(amplitude)
Rhythm retained (Dec1 f/f)
Rhythm disrupted (Dec1 f/f)
Rhythm acquired (Dec1 βKO)
Rhythm shifted (Dec1 f/f)
Rhythm shifted (Dec1 βKO)
B
Rhythm
Shifted
Gained
Disrupted
% bound by DEC1
C
Dec1f/f
Dec1 βKO
Rhythm shifted phase
E
Glucose-stimulated insulin secretion
Dynll1
Gnaz
Syn1
Gnai2
Hif1a
Gnaq
Entpd1
Gnas
Syt13
Nr1d1
Irs1
Syt4
Slc2a2
Irs2
Igf1
Itgam
PI3K-Akt-mTOR signaling
Runx1
Gnai2
Pik3r1
Itgb1
Adcy4
Foxo1
Gnb1
Calm3
Gng4
Gsk3b
COPI complex | vesicle-mediated transport
Copz2
Racgap1
Tubb3
Nbas
Gbf1
Arf3
Tmed3
Surf4
Tuba1b
Arfgap1
Phase shift (hr)
D
Magnitude
Dec1f/f phase (hr)
Dec1 βKO phase (hr)
Insulin Secretion
Abr
Gnaz
Adora1
Gnai2
Rest
Ffar2
Pfkl
Foxo1
Entpd1
Nos1
Madd
Ptpn11
C9orf72
Acsl4
Irs1
Syt4
Fmr1
ATPase-coupled Ca2+ transport
Scn1b
Amigo1
Tlr9
Pde4b
Ank2
Itgb1
Ptm1
Dapk1
1810037I17Rik
App
Fhl1
Calm3
Prnp
Cltrn
Rasgrf1
Mrln
Cftr
Fmr1
Ppp3cb
TCA cycle | respiratory electron chain
Hspa8
mt−Nd2
mt−Nd1
Nudt5
mt−Nd4
mt−Nd5
mt−Nd3
mt−Nd6
mt−Atp8
Pkm
Atp5h
ATPase-coupled Ca2+ transport
Cellular response to stimuli
COPI complex | vesicle-mediated transport
Glucose-stimulated insulin secretion
Insulin Secretion
PI3K-Akt-mTOR signaling
Protein kinase signaling
STK activity
TCA cycle | respiratory electron chain
F
Clock
Nr1d1
Nr1d2
Npas2
Cry1
Cry2
Per1
Per2
log2(normalized counts)
Time (hr)
Dec1f/f
Dec1 βKO
G
mt-Nd2
Vamp2
Snap25
Unc13a
Stxbp2

**Figure S5. DEC1 coordinates β-cell respiratory metabolism and insulin secretion gene rhythms.**

(**A**) Distribution of rhythm amplitudes for genes whose expression rhythm is disrupted (left), enhanced (middle), and shifted (right) in *Dec1 βKO* mice, compared to those of rhythm-retaining genes.

(**B**) Proportion of genes whose expression rhythm is disrupted, enhanced, or shifted in *Dec1 βKO* mice that is bound by DEC1 in β cells.

(**C**) Phase distribution of transcripts whose expression rhythm is shifted in *Dec1 βKO* mice.

(**D**) Magnitude and phase of enriched pathways among genes whose expression rhythm is shifted in *Dec1 βKO* mice, colored by biological theme.

(**E**) Phase change for genes whose expression rhythm is shifted in *Dec1 βKO* mice, grouped and colored by biological theme.

(**F-G**) Examples of genes with unaltered (F) and altered (G) temporal expression patterns in *Dec1 βKO* mice.

Data are mean from n =4 replicate measurements of islets isolated and pooled from N =2 *Dec1-βKO* and 2 littermate control mice.

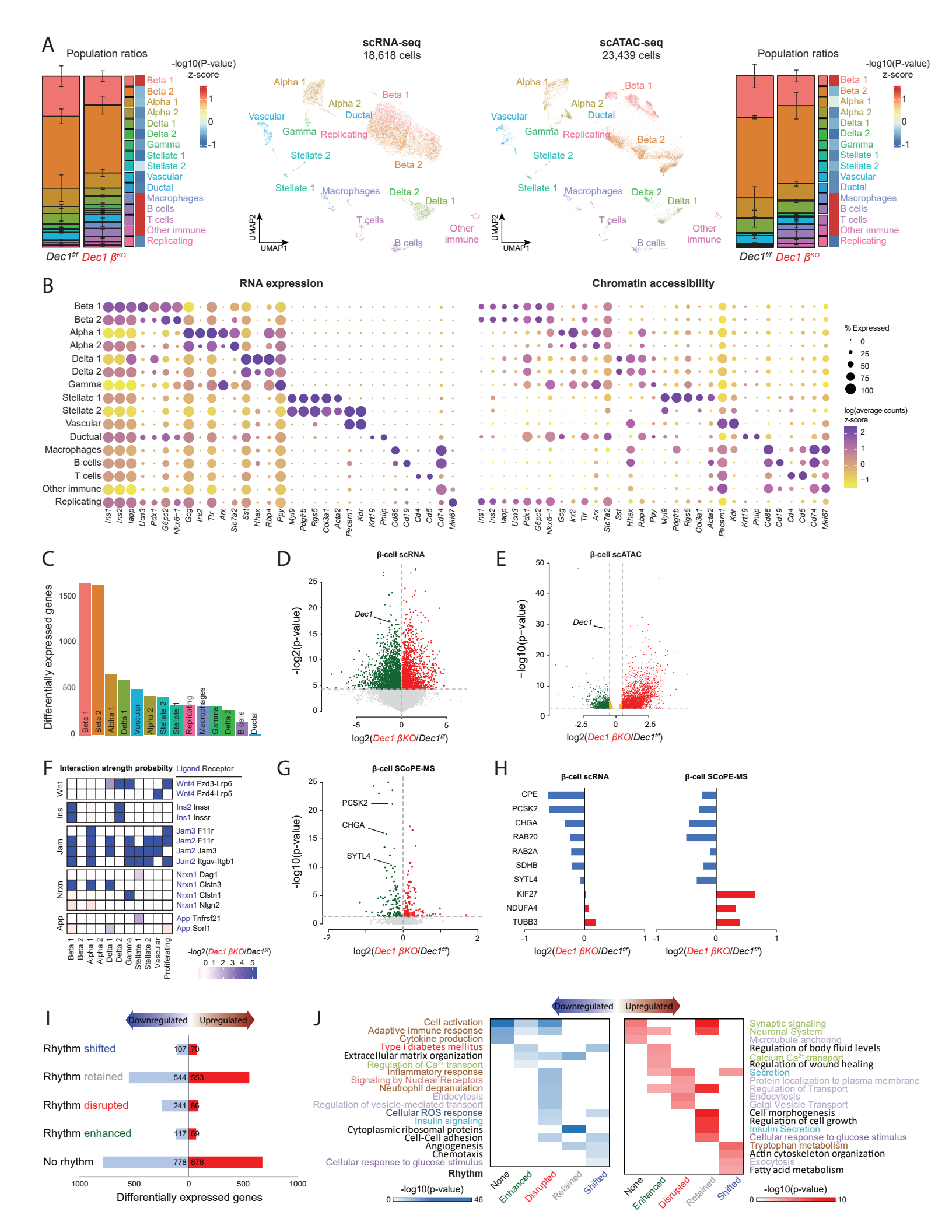
A
Population ratios
-log10(P-value)
z-score
Beta 1
Beta 2
Alpha 1
Alpha 2
Delta 1
Delta 2
Gamma
Stellate 1
Stellate 2
Vascular
Ductal
Macrophages
B cells
T cells
Other immune
Replicating
Dec1f/f
Dec1 βKO
scRNA-seq
18,618 cells
scATAC-seq
23,439 cells
UMAP1
UMAP2
B
RNA expression
Chromatin accessibility
% Expressed
log(average counts)
z-score
C
Differentially expressed genes
D
β-cell scRNA
-log2(p-value)
log2(Dec1 βKO/Dec1f/f)
E
β-cell scATAC
−log10(p−value)
F
Interaction strength probabilty
Ligand Receptor
Wnt4 Fzd3-Lrp6
Wnt4 Fzd4-Lrp5
Ins2 Insr
Ins1 Insr
Jam3 F11r
Jam2 F11r
Jam2 Jam3
Jam2 Itgav-Itgb1
Nrxn1 Dag1
Nrxn1 Clstn3
Nrxn1 Clstn1
Nrxn1 Nlgn2
App Tnfrsf21
App Sorl1
Proliferating
G
β-cell SCoPE-MS
-log10(p-value)
PCSK2
CHGA
SYTL4
H
CPE
RAB20
RAB2A
SDHB
KIF27
NDUFA4
TUBB3
I
Downregulated
Upregulated
Rhythm shifted
Rhythm retained
Rhythm disrupted
Rhythm enhanced
No rhythm
Differentially expressed genes
J
Cell activation
Adaptive immune response
Cytokine production
Type I diabetes mellitus
Extracellular matrix organization
Regulation of Ca2+ transport
Inflammatory response
Signaling by Nuclear Receptors
Neutrophil degranulation
Endocytosis
Regulation of vesicle-mediated transport
Cellular ROS response
Insulin signaling
Cytoplasmic ribosomal proteins
Cell-Cell adhesion
Angiogenesis
Chemotaxis
Cellular response to glucose stimulus
Rhythm
None
Enhanced
Disrupted
Retained
Shifted
-log10(p-value)
Synaptic signaling
Neuronal System
Microtubule anchoring
Regulation of body fluid levels
Calcium Ca2+ transport
Regulation of wound healing
Secretion
Protein localization to plasma membrane
Regulation of Transport
Endocytosis
Golgi Vesicle Transport
Cell morphogenesis
Regulation of cell growth
Insulin Secretion
Cellular response to glucose stimulus
Tryptophan metabolism
Actin cytoskeleton organization
Exocytosis
Fatty acid metabolism

**Figure S6. Chromatin, transcription, and protein level deregulation of glucose metabolism and glucose-dependent insulin secretion in β-cells of *Dec1-βKO* mice.**

(**A)** Single-cell clustering by gene expression profiles (left, scRNA-seq) and by open chromatin profiles (right, scATAC-seq) in islets isolated from N =2 *Dec1-βKO* and 2 littermate control mice, each sequenced separately, with population ratios and the relative significance of ratio changes (hypergeometric test) shown to the sides.

(**B**) Quantification of RNA (left) and open chromatin (right) reads mapping to select marker genes for each cell cluster in (A). Color represents z-normalized average read counts, and diameter denotes fractional expression.

(**C**) Distribution of genes that are differentially expressed in the indicated cell types in islets isolated from either or both of N =2 *Dec1-βKO* relative to 2 littermate control mice, each sequenced separately.

(**D-E**) Changes in gene expression (D) and chromatin accessibility (E) in β-cells pooled from N =2 *Dec1-βKO* relative to 2 littermate control mice, each sequenced separately.

(**F**) Changes in intercellular ligand-receptor interaction strength probabilities in islets pooled from N =2 *Dec1-βKO* relative to 2 littermate control mice, for 7 of the top 10 differentially active interactions where the ligand expression is significantly altered in Beta 1 cells (β cells with higher expression of insulin and maturity markers), based on scRNA-seq data. Grouped ligand-receptor pairs are indicated to the right.

(**G-H**) Proteome changes in β-cells pooled from N =2 *Dec1-βKO* relative to 2 littermate control mice, each run separately (G). RNA and protein changes in β-cells for selected targets are shown in (H).

(**I**) Distribution of genes differentially expressed in β-cells pooled from N =2 *Dec1-βKO* and 2 littermate control mice, each run separately, among non-rhythmic or enhanced, disrupted, retained, or shifted rhythmicity models.

(**J**) Pathways enriched among non-rhythmic genes or genes with enhanced, disrupted, retained, or shifted rhythmicity that are downregulated (left) or upregulated (right) in β-cells pooled from N =2 *Dec1-βKO* and 2 littermate control mice, each run separately

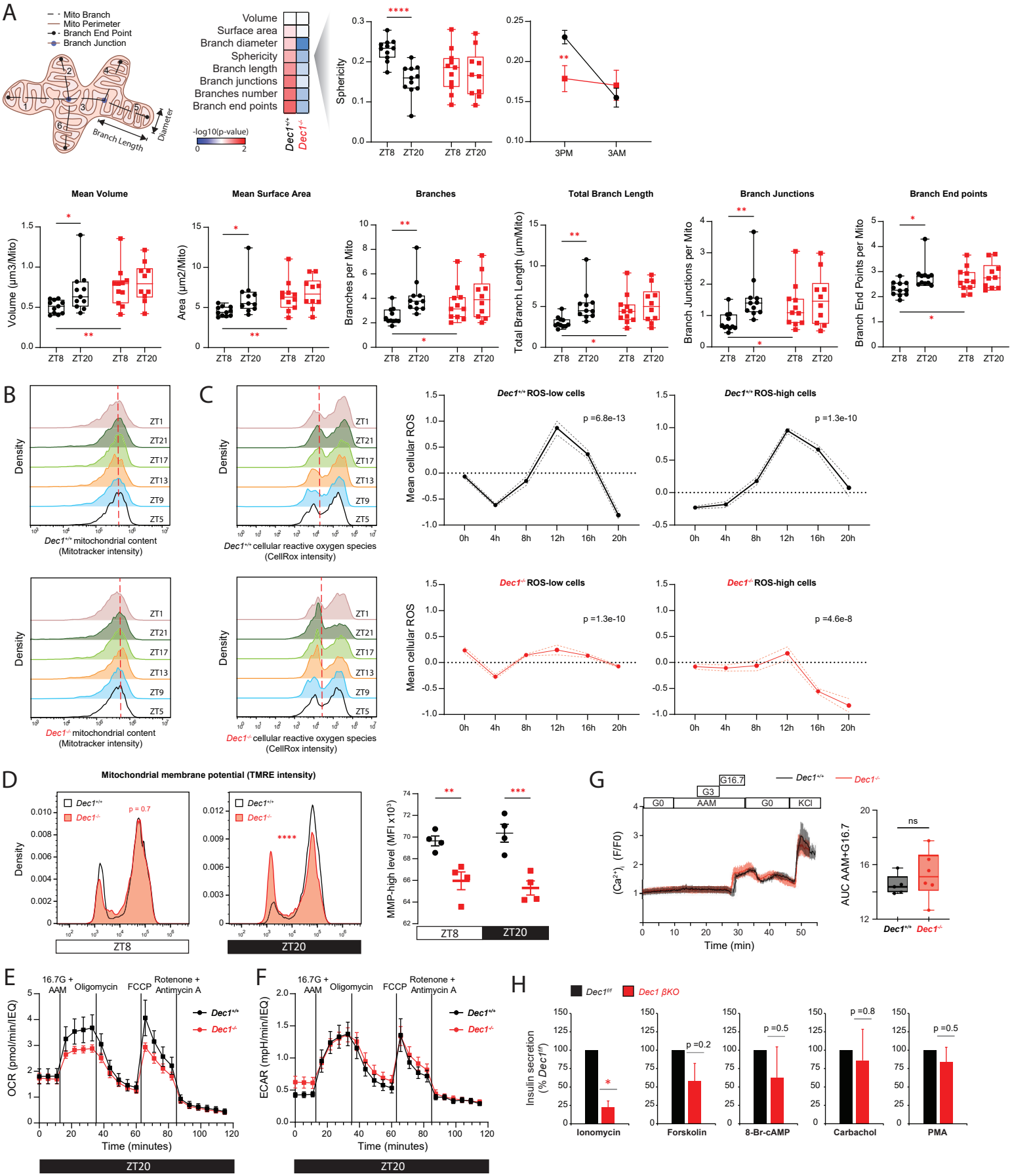
A
Mito Branch
Mito Perimeter
Branch End Point
Branch Junction
Branch Length
Diameter
Volume
Surface area
Branch diameter
Sphericity
Branch length
Branch junctions
Branches number
Branch end points
-log10(p-value)
Dec1+/+
Dec1-/-
Sphericity
ZT8
ZT20
3PM
3AM
Mean Volume
Mean Surface Area
Branches
Total Branch Length
Branch Junctions
Branch End points
Volume (µm3/Mito)
Area (µm2/Mito)
Branches per Mito
Total Branch Length (µm/Mito)
Branch Junctions per Mito
Branch End Points per Mito
B
C
Density
ZT1
ZT21
ZT17
ZT13
ZT9
ZT5
Dec1+/+ mitochondrial content
(Mitotracker intensity)
Dec1+/+ cellular reactive oxygen species
(CellRox intensity)
Dec1-/- mitochondrial content
(Mitotracker intensity)
Dec1-/- cellular reactive oxygen species
(CellRox intensity)
Dec1+/+ ROS-low cells
Dec1+/+ ROS-high cells
Dec1-/- ROS-low cells
Dec1-/- ROS-high cells
Mean cellular ROS
p =6.8e-13
p =1.3e-10
p =1.3e-10
p =4.6e-8
0h
4h
8h
12h
16h
20h
D
Mitochondrial membrane potential (TMRE intensity)
Dec1+/+
Dec1-/-
p = 0.7
MMP-high level (MFI x10³)
ZT8
ZT20
G
G16.7
G3
G0
AAM
KCl
(Ca²⁺)i (F/F0)
Time (min)
AUC AAM+G16.7
ns
E
16.7G + AAM
Oligomycin
FCCP
Rotenone + Antimycin A
OCR (pmol/min/IEQ)
Time (minutes)
F
ECAR (mpH/min/IEQ)
H
Dec1f/f
Dec1 βKO
Insulin secretion (% Dec1f/f)
Ionomycin
Forskolin
8-Br-cAMP
Carbachol
PMA
p =0.2
p =0.5
p =0.8
p =0.5

**Figure S7. Disruption of circadian mitochondrial dynamics and energy metabolism underlies immature β-cell function upon DEC1 loss.**

(**A**) Mitochondrial structural features (left) quantified by confocal imaging of MitroTracker Red CMXRos staining in β-cells isolated from *Dec1*$^{+/+}$ and *Dec1*$^{-/-}$ mice assayed every 4h for 20h, and their 24h rhythmicity significance (RAIN) (center). Diagram skeletonizes a mitochondrion to mark 6 branches (1-6), 5 branch end points, and 2 branch junctions, and shows the perimeter used to calculate volume and sphericity. Quantifications at ZT8 and ZT20 of the indicated structural features are shown to the right and below. Data are distributions and mean ±SEM of imaging measurements from n =10 independent fields of view.

(**B**) Mitochondrial content across β-cells isolated from *Dec1*$^{+/+}$ and *Dec1*$^{-/-}$ mice, assayed by MitoTracker Green fluorescence intensity at 4h intervals for 20h.

(**C**) Cellular reactive oxygen species (ROS) distributions (left) and their 24h rhythmicity analysis (middle and right) in β-cells isolated from *Dec1*$^{+/+}$ and *Dec1*$^{-/-}$ mice. Distributions display flow cytometry of CellRox Deep Red intensity in β-cells analyzed every 4h for 20h, with separation of ROS-low and -high populations in the initial (0h) timepoint indicated. Rhythmicity analysis quantifies detrended (baseline-subtracted) mean ± SEM intensity for ROS-low and -high cell populations separately. Rhythmicity p-value, RAIN.

(**D**) Mitochondrial membrane potential (MMP) across β-cells isolated from *Dec1*$^{+/+}$ and *Dec1*$^{-/-}$ mice (left and center), determined by TMRE staining at ZT8 and ZT20, and quantification of mean fluorescence intensity (MFI) for MMP-high cells (right). Data are distributions and mean values from n=4 replicate measurements, each with >10,000 cells.

(**E-F**) Metabolic flux at ZT20 in islets isolated from *Dec1*$^{+/+}$ and *Dec1*$^{-/-}$ mice quantified from measurements of oxygen consumption rate (OCR) (E) and extracellular acidification rate (ECAR) (F) in response to 16.7mM glucose and a physiological amino acid mixture (16.7G + AAM), oligomycin, FCCP, and to rotenone and antimycin A at the indicated times. Data are mean ±SEM from n =4-6 replicate measurements of 12 similar-sized islets.

(**G**) $Ca^{2+}$ influx measured by Fura-2 staining in response to no glucose (G0), a physiological mixture of amino acids (AAM), AAM supplemented with 3mM glucose (G3), AAM supplemented with 16.7mM glucose (G16.7), no glucose, and 30mM KCl, with influx during AAM+G16.7 quantified to the right.

(**H**) Glucose and secretagogue-stimulated insulin secretion in size-matched islets isolated from N =4-5 *Dec1*-βKO and 4-6 littermate control mice, each with n =2-3 replicate measurements, normalized to intracellular insulin content. Data are mean ±SEM.